AGU PUBLICATIONS

JGR

Journal of Geophysical Research: Biogeosciences

RESEARCH ARTICLE
10.1002/2014JG002888

This article is a companion to *Grant* [2015] doi:10.1002/2014JG002889.

Key Points:
- NEP of drier upland tundra does not rise much in warmer years
- NEP of lowland fen rises in warmer years
- CH_4 is emitted by degassing with summer warming and autumn freezing

Supporting Information:
- Supporting Information S1

Correspondence to:
R. F. Grant,
rgrant@ualberta.ca

Citation:
Grant, R. F., E. R. Humphreys, and P. M. Lafleur (2015), Ecosystem CO_2 and CH_4 exchange in a mixed tundra and a fen within a hydrologically diverse Arctic landscape: 1. Modeling versus measurements, *J. Geophys. Res. Biogeosci.*, *120*, 1366–1387, doi:10.1002/2014JG002888.

Received 16 DEC 2014
Accepted 18 JUN 2015
Accepted article online 23 JUN 2015
Published online 24 JUL 2015

Ecosystem CO_2 and CH_4 exchange in a mixed tundra and a fen within a hydrologically diverse Arctic landscape: 1. Modeling versus measurements

R. F. Grant[1], E. R. Humphreys[2], and P. M. Lafleur[3]

[1]Department of Renewable Resources, University of Alberta, Edmonton, Alberta, Canada, [2]Department of Geography, Carleton University, Ottawa, Ontario, Canada, [3]Department of Geography, Trent University, Peterborough, Ontario, Canada

Abstract CO_2 and CH_4 exchange are strongly affected by hydrology in landscapes underlain by permafrost. Hypotheses for these effects in the model *ecosys* were tested by comparing modeled CO_2 and CH_4 exchange with CO_2 fluxes measured by eddy covariance from 2006 to 2009, and with CH_4 fluxes measured with surface chambers in 2008, along a topographic gradient at Daring Lake, NWT. In an upland tundra, rises in net CO_2 uptake in warmer years were constrained by declines in CO_2 influxes when vapor pressure deficits (D) exceeded 1.5 kPa and by rises in CO_2 effluxes with greater active layer depth. Consequently, net CO_2 uptake rose little with warming. In a lowland fen, CO_2 influxes declined less with D and CO_2 effluxes rose less with warming, so that rises in net CO_2 uptake were greater than those in the tundra. Greater declines in CO_2 influxes with warming in the tundra were modeled from greater soil-plant-atmosphere water potential gradients that developed under higher D in drained upland soil, and smaller rises in CO_2 effluxes with warming in the fen were modeled from O_2 constraints to heterotrophic and belowground autotrophic respiration from a shallow water table in poorly drained lowland soil. CH_4 exchange modeled during July and August indicated very small influxes in the tundra and larger effluxes characterized by afternoon emission events caused by degassing of warming soil in the fen. Emissions of CH_4 modeled from degassing during soil freezing in October–November contributed about one third of the annual total.

1. Introduction

The hydrology of Arctic tundra is strongly affected by poor drainage in landscapes underlain by impermeable permafrost. The consequent redistribution of surface and near-surface water along topographic gradients causes large spatial variation in soil water contents (θ) and plant functional types (PFTs) within tundra landscapes which affect ecosystem productivity [*Sturtevant and Oechel*, 2013].

In higher topographic positions from which water is shed, lower θ reduces soil heat capacity which enables earlier soil warming that may hasten early season productivity relative to that in lower topographic positions [*Hodkinson et al*., 1999]. However, lower θ may also cause productivity in higher topographic positions to be more adversely affected by water stress and consequent lower stomatal conductance (g_c) under higher air temperatures (T_a) and vapor pressure deficits (D) during warming events later in the growing season [*Williams et al*., 2000].

In lower topographic positions where water gathers, high θ reduces heterotrophic respiration (R_h) relative to that at higher topographic positions. This reduction is caused by slower O_2 uptake by aerobic heterotrophs, and hence slower redox reactions driven by O_2 reduction, forcing alternative redox reactions with smaller energy yields (e.g., methanogenesis). The consequent slowing of soil C oxidation and hence of soil nutrient mineralization and plant nutrient uptake reduces gross primary productivity (GPP) and hence net primary productivity (NPP) relative to those at higher topographic positions. However, the reduction of NPP in lower versus higher topographic positions is thought to be less than that in R_h so that net ecosystem productivity (NEP = NPP − R_h) in lower positions may be greater. These different effects of θ on NPP and R_h may explain the smaller R_h but larger NEP of wet-sedge versus moist-tussock tundra found by *Vourlitis et al*. [2000].

These different effects of θ on R_h and productivity with topographic position may also determine the responses of different tundra types to warming. *Oberbauer et al*. [2007] found that experimental warming

of wet-sedge tundra caused greater increases in CO_2 uptake than in CO_2 emission, which they attributed to constraints on ecosystem respiration (R_e) from high θ. In contrast, they found that experimental warming of drier tundra frequently caused greater increases in CO_2 emission than in CO_2 uptake and in some cases caused decreases in CO_2 uptake. *Marchand et al.* [2005] also found that experimental warming of a grassland tundra raised R_e more than CO_2 fixation, thereby reducing net CO_2 uptake. These contrasting responses of net CO_2 exchange to warming in wet and dry tundra may explain results from the meta-analysis of *Elmendorf et al.* [2012] in which experimental warming increased total shrub abundance at moist and wet sites but decreased it at dry sites. Warming effects on ecosystem function were generally found to increase linearly with duration of warming for up to 20 years (the maximum included in the meta-analysis) but occasionally to cease or decline with time (transient effects) [*Elmendorf et al.*, 2012]. Consequently, there is strong evidence that responses in net CO_2 exchange and productivity of tundra ecosystems to warming over time will depend upon their hydrology as determined by their topographic positions.

Changes in productivity of Arctic ecosystems with long-term climate warming are often projected by process-based models with inputs for weather, soil attributes, and plant functional types (PFTs) for Arctic regions [e.g., *McGuire et al.*, 2012; *Zhu et al.*, 2013]. However, these projections need to be supported by well-constrained tests of changes in productivity of diverse Arctic ecosystems modeled under ambient changes in weather at diurnal, seasonal, and annual time scales. Such tests require that models represent landscape hydrology and its effects on key processes governing C, O_2, water, heat, and nutrient transformations and transfers that determine NPP and R_h [e.g., *Miller and Smith*, 2012]. Most models currently used for such projections do not represent landscape hydrology, lack well-tested nutrient cycles, and usually function at time steps (e.g., monthly) that are much longer than those of hydrological effects on these key processes (e.g., hourly) that determine productivity. Consequently, these models are capable of only poorly constrained tests against temporally aggregated observations of weather and productivity.

There is a need for future projections of climate change impacts on Arctic productivity to be based on models in which a comprehensive set of processes governing C, O_2, water, heat, and nutrient transformations and transfers that drive ecosystem productivity are fully coupled with landscape hydrology at appropriate time steps and so are capable of better constrained tests. Here we implement and test this coupling in the ecosystem model *ecosys*, in which a comprehensive set of fully coupled biological and hydrological processes has been extensively tested against eddy covariance fluxes and related ecophysiological measurements under contrasting site and weather conditions in boreal, temperate, and tropical forests [*Grant et al.*, 2007b, 2007c, 2009a, 2009b, 2009c, 2010]; wetlands [*Dimitrov et al.*, 2011, 2014; *Grant and Roulet*, 2002; *Grant et al.*, 2012b; *Mezbahuddin et al.*, 2014]; grasslands [*Grant and Flanagan*, 2007; *Grant et al.*, 2012a]; tundra [*Grant et al.*, 2003, 2011a]; and croplands [*Grant et al.*, 2007a, 2011b].

A unique opportunity to test the modeled effects of differences in hydrology on ecosystem productivity under ambient changes in weather was provided by concurrent multiyear measurements of CO_2 and energy exchange by eddy covariance (EC) over a mixed tundra and a fen within the same watershed at Daring Lake, NWT [*Humphreys and Lafleur*, 2011]. We will determine whether model hypotheses for these coupled biological and hydrological processes, functioning under contrasting hydrological conditions, explain different responses of CO_2 and CH_4 exchange to changes in weather observed in these distinct tundra types. Based on earlier findings [*Humphreys and Lafleur*, 2011], these different responses and their proposed explanations include

1. net C uptake is more adversely affected by short-term warming in mixed tundra than in fen because CO_2 fixation in mixed tundra is more limited by g_c.
2. R_e rises more during short-term warming in mixed tundra than in fen because R_h and belowground R_a in fen are limited more by soil O_2 than are those in mixed tundra.
3. therefore, short-term warming should raise net C uptake more in fen than in mixed tundra, and
4. O_2 limitations in fen causes more products of R_h to be emitted as CH_4 than in mixed tundra, offsetting any gains in net C uptake in terms of greenhouse gas equivalents.

We test these explanations by conducting detailed comparisons of modeled energy and CO_2 exchange against EC measurements over a drier upland mixed tundra and a wetter lowland fen with contrasting hydrological conditions caused by different topographical positions within a common landscape. These comparisons

are conducted under contrasting weather conditions over 5 years (2005–2009) and are supported by concurrent tests of modeled changes in active layer depths (ALDs) and of CH_4 emissions against measurements at both sites.

2. Model Description

The key algorithms governing the simulation of hydrological controls on C and N transformations in *ecosys* are described in the supporting information to this article, in which equations and variables referenced in the Results and Discussion section below are described and listed in Appendices A through H in the supporting information. Algorithms representing biological processes of diverse microbial communities in soil, including aerobic (bacteria and fungi); facultative anaerobic (denitrifiers); and anaerobic (fermenters, and acetotrophic methanogens), heterotrophs, and autotrophs (nitrifiers, methanotrophs, and hydrogenotrophic methanogens), are presented in Appendix A: Microbial C, N, and P transformations; Appendix G: CH_4 production and consumption; and Appendix H: Inorganic N transformations. Physical processes driving soil-plant-atmosphere water transfer using coupled algorithms for hydraulically driven root water uptake with energy-driven canopy transpiration are presented in Appendix B: Soil-plant water relations. Biological processes driving C, N, and P transformations in multispecies plant communities using biochemically based algorithms for C fixation, transport, transformation, and respiration are presented in Appendix C: Gross primary productivity, autotrophic respiration, growth, and litterfall and in Appendix F: Symbiotic N_2 fixation. Chemical processes governing soil solute transformations including precipitation-dissolution, adsorption-desorption, and ion-pairing equilibria are presented in Appendix E: Solute transformations. All these algorithms were solved at an hourly time step from hourly changes in atmospheric boundary conditions. Physical processes driving soil water, heat, and solute transfers using partial differential and convective-dispersive algorithms are presented in Appendix D: Soil water, heat, gas, and solute fluxes. Algorithms for water, heat, and solute fluxes were solved at a 4 min time step, within which those driving gas transfers were solved at an 8 s time step, assuming constant boundary conditions during each hour. All parameters in these algorithms remained unchanged from those in earlier studies of forests, crops, and grasslands cited in this paper. The key model hypotheses for hydrological controls on heterotrophic respiration (R_h) (Appendix A), autotrophic respiration (R_a), and gross primary productivity (GPP) (Appendix C) are further described and tested for dryland sites in *Grant et al.* [2012a] and for wetland sites in *Grant et al.* [2012b]. Model hypotheses for hydrological controls on CH_4 production and oxidation (Appendix G) are further described and tested in *Grant* [1998, 1999] and in *Grant and Roulet* [2002]. These hypotheses are summarized in flow diagrams for aerobic and anaerobic heterotrophic transformations in Figure 1 of *Grant* [1998] and for hydrological controls on gaseous and aqueous transport of the substrates and products of these transformations in Figure 1 of *Grant and Pattey* [2008].

3. Methods

3.1. Site Description

The mixed tundra and fen sites were located within an ~1 km wide, shallow valley draining to the southwest into Daring Lake (64°52′N, 111°35′W) in the central Northwest Territories in Canada's Southern Arctic Ecozone. The fen site was a 48 ha wet-sedge meadow extending along the bottom of the valley, characterized by a fluctuating water table ±10 cm from the moss surface, with 40 to 70 cm of peat over a silt loam mineral soil. The mixed tundra site was located approximately 0.5 km upslope (1°) to the NW of the fen and was characterized by a topography-driven heterogeneous mix of two broad tundra types, mesic heath and shrub tussock tundra with approximately equal fractional coverage within the tower flux footprint. The organic layer ranged from 1 to 22 cm in depth over coarse textured mineral soil (sand to loamy sand). Key soil properties at both sites are summarized in Table 1. The sites are further described in *Humphreys and Lafleur* [2011] and in *Lafleur and Humphreys* [2008].

3.2. Site Measurements

The eddy covariance (EC) technique was used to measure CO_2 and energy fluxes at both sites during growing seasons from 2004 (mixed tundra) or 2006 (fen) to 2009. Net CO_2 exchange was computed as the sum of the turbulent CO_2 flux and the rate of change in storage of CO_2 below the height of the instrumentation. The EC methodology is further described in *Lafleur and Humphreys* [2008]. Methane emissions were recorded during 2008 along a transect across the fen with a 0.0219 m^3 opaque static,

Table 1. Key Soil Properties of the (a) Mixed Tundra and (b) Fen Sites at Daring Lake Used in *Ecosys*

Depth	BD	TOC[a]	TON[b]	C:N	FC[c]	WP[c]	K_{sat}[c]	pH	Sand[d]	Silt[d]	Clay[d]
(a) Mixed tundra											
m	$mg\ m^{-3}$	$g\ kg^{-1}$	$g\ kg^{-1}$		$m^3\ m^{-3}$	$m^3\ m^{-3}$	$mm\ h^{-1}$		$g\ kg^{-1}$	$g\ kg^{-1}$	$g\ kg^{-1}$
0.01	0.174	415	11.86	35	0.45	0.15	200	6.2	800	160	40
0.035	0.174	415	11.86	35	0.45	0.15	200	6.2	800	160	40
0.065	0.362	176	7.04	25	0.3	0.1	200	6.2	800	160	40
0.135	0.693	50	2.50	20	0.25	0.1	200	6.2	800	160	40
0.25	1.122	45	2.25	20	0.25	0.1	200	6.2	800	160	40
0.375	1.39	28	1.40	20	0.25	0.1	200	6.2	800	160	40
0.51	1.394	35	1.75	20	0.25	0.1	200	6.2	800	160	40
0.68	1.42	5.5	0.37	15	0.16	0.065	100	6.2	800	160	40
0.80	1.52	6.3	0.42	15	0.16	0.065	100	6.2	800	160	40
1.30	1.52	2	0.13	15	0.16	0.065	100	6.2	800	160	40
1.80	1.52	1	0.07	15	0.16	0.065	100	6.2	800	160	40
2.80	1.52	1	0.07	15	0.16	0.065	100	6.2	800	160	40
(b) Fen											
m	$mg\ m^{-3}$	$g\ kg^{-1}$	$g\ kg^{-1}$		$m^3\ m^{-3}$	$m^3\ m^{-3}$	$mm\ h^{-1}$		$g\ kg^{-1}$	$g\ kg^{-1}$	$g\ kg^{-1}$
0.01	0.021	500	20	25	0.15	0.025	500	6.2	83	689	228
0.035	0.021	500	20	25	0.15	0.025	500	6.2	83	689	228
0.065	0.050	500	20	25	0.3	0.05	150	6.2	83	689	228
0.135	0.068	500	25	20	0.35	0.075	75	6.2	83	689	228
0.25	0.112	500	25	20	0.52	0.12	25	6.2	83	689	228
0.375	0.179	500	25	20	0.73	0.19	25	6.2	83	689	228
0.51	0.184	500	25	20	0.73	0.19	25	6.2	83	689	228
0.68	1.42	5.5	0.367	15	0.283	0.108	15	6.2	83	689	228
0.80	1.52	6.3	0.42	15	0.283	0.108	15	6.2	83	689	228
1.30	1.52	2	0.133	15	0.283	0.108	15	6.2	83	689	228
1.80	1.52	1	0.067	15	0.283	0.108	15	6.2	83	689	228
2.80	1.52	1	0.067	15	0.283	0.108	15	6.2	83	689	228

[a]Abbreviations BD: bulk density, TOC and TON: total organic C and N, FC: field capacity, WP: wilting point, K_{sat}: saturated hydraulic conductivity.
[b]Calculated from C:N ratios measured in comparable soils by *Ping et al*. [1998].
[c]Values for organic layers were derived from generalized relationships in *Boelter* [1969] and *Päivänen* [1973] and those in mineral layers from pedotransfer functions in *Saxton et al*. [1986].
[d]Sand, silt, and clay contents were recalculated in *ecosys* to account for SOC and coarse fragments. Values below 1 m assumed the same as those measured above.

nonsteady state surface chamber in which CH_4 concentrations were measured with a gas chromatograph (CP 3800, Varian, CA) equipped with a flame-ionization detector. The CH_4 measurement methodology is further described in *Wilson and Humphreys* [2010].

3.3. Model Experiment

3.3.1. Soils and Hydrology

The Daring Lake landscape was represented in *ecosys* as a transect consisting of six interconnected segments of 200 m × 200 m on a slope with a SE aspect declining from 1° to 0° while approaching an external water table representing Daring Lake (Figure 1). The depth of the external water table with respect to the lowest segment was set to allow the depth of the water table in the segment representing the modeled fen site to remain within a few centimeters of the fen surface, consistent with a water table observed to remain within 10 cm of the moss surface at the Daring Lake fen site [*Humphreys and Lafleur*, 2011]. The elevation of the mixed tundra landscape positions above the external water table (Figure 1) caused the mixed tundra to shed water, and the fen to gather water, whenever lateral surface and subsurface flows from the mixed tundra down to the fen were modeled. These flows allowed drying and rewetting of near-surface soil which enabled θ modeled in the mixed tundra to follow that measured during the growing seasons of 2008 and 2009 ($R^2 = 0.72$, root-mean-square deviation (RMSD) = 0.03 $m^3\ m^{-3}$). These flows eventually drove discharge from the shallow water table in the boundary fen to the external water table in Daring Lake. Water table dynamics used to simulate wetland hydrology in *ecosys* are described elsewhere [*Grant et al*., 2012b; *Mezbahuddin et al*., 2014]. Key properties used to represent the soils in each landscape segment (Table 1) were taken from analyses of soil samples or derived from pedotransfer functions. The second

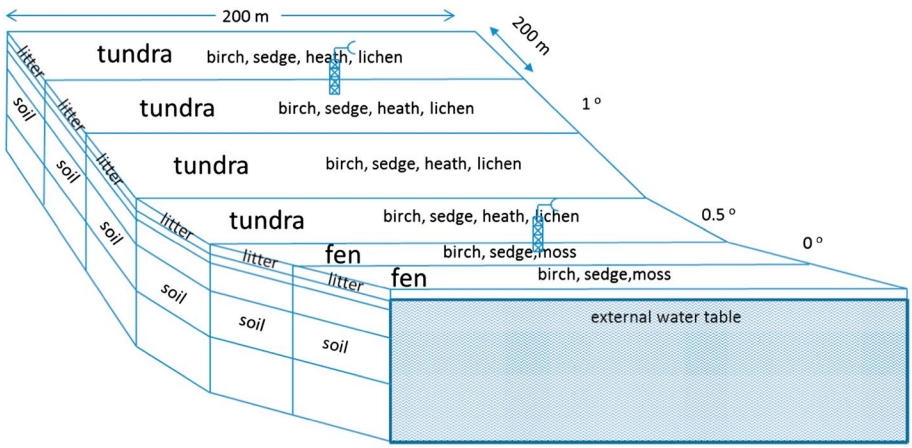

Figure 1. Transect at Daring Lake as modeled in *ecosys* showing grid cells with soil types and plant species used to represent fetch areas of the flux towers in the mixed tundra and fen.

upper and second lower segments of the transect were used to represent the fetches of the flux towers at the mixed tundra and fen sites, respectively (Figure 1).

3.3.2. Plant Functional Types

Plant species used to represent vegetative communities for the mixed tundra (segments 1–4) and fen (segments 5 and 6) were taken from those given in site descriptions by *Humphreys and Lafleur* [2011] and *Lafleur et al*. [2012] and modeled as PFTs. Birch was modeled as a flood-tolerant dwarf deciduous tree (larger leaf specific area, N and P contents, full annual leaf turnover, and large root aerenchyma in *Grant et al*. [2009c, 2011a]), sedge as a wetland grass (larger leaf specific area, N and P contents, full annual aboveground turnover, and large root aerenchyma in *Grant et al*. [2012b]), heath as a needleleaf semideciduous shrub (smaller leaf specific area, N and P contents, partial annual leaf turnover, and smaller root aerenchyma in *Grant et al*. [2009c, 2011a]), and moss and lichen as nonvascular semideciduous plants (smaller leaf specific area, N and P contents, partial annual leaf turnover, no aerenchyma, and no stomatal response in *Dimitrov et al*. [2011]). The moss and lichen were associated with N_2-fixing cyanobacterial populations which exchanged nonstructural N for nonstructural C and P with the host plants as described in Appendix F1–F26. The biological properties of these PFTs were the same as those used in earlier modeling studies of boreal forests and wetlands [e.g., *Grant et al*., 2009c, 2012b] but with shortened internode lengths to reproduce the dwarf stature of the shrubs at Daring Lake [*Grant et al*., 2011a]. Because vertical profiles of canopy leaf area and root lengths are explicitly modeled from allocations of plant nonstructural C (C20 and C21), each PFT competes for irradiance, water, and nutrients within each canopy and rooted soil layer according to its vertical distributions of leaf area and root length driven by its growth.

3.3.3. Model Run

Site history was simulated by running *ecosys* with these landscape PFTs and soil properties for model years from 1 January 1907 to 31 December 2009 under repeating 6 year sequences of hourly-averaged weather data (radiation, T_a, relative humidity, wind speed, and precipitation) recorded at Daring Lake from 1 January 2004 to 31 December 2009. During this period, atmospheric CO_2 concentrations (C_a) rose at 0.3% y^{-1} from 280 to 380 μmol mol^{-1} and concentrations of NH_4^+ and NO_3^- in precipitation of 0.125 g N m^{-3} gave N deposition rates reported in *Environment Canada* [2004]. This spin-up allowed the model to attain stable values for CO_2 and energy exchange during successive sequences of weather data for several decades before its termination. Model results for CO_2 and energy fluxes from the second upper and lower segments of the landscape were then compared with those measured at EC towers in the mixed tundra and fen. Model results for CH_4 emissions from the fen segments were compared with those measured in the fen by *Wilson and Humphreys* [2010].

In an accompanying paper [*Grant*, 2015], this model run was extended from 2010 to 2110 under a climate change scenario generated by a regional circulation model. Separate runs were conducted for (1) no

Table 2. Statistics From Regressions of Simulated on Measured Hourly CO_2 Fluxes Over Arctic Mixed Tundra and Fen Sites at Daring Lake, NWT[a]

		a[b]			RMSD[c]	RMSE[d]
	N	$\mu mol\ m^{-2}\ s^{-1}$	b[b]	R^2	$\mu mol\ m^{-2}\ s^{-1}$	$\mu mol\ m^{-2}\ s^{-1}$
				Mixed Tundra		
2005	1716	0.03	1.15	0.83	0.54	0.61
2006	2949	0.01	1.09	0.72	0.70	0.62
2007	1619	0.15	1.04	0.81	0.72	0.69
2008	1963	−0.01	0.92	0.76	0.82	0.67
2009	2720	−0.15	1.07	0.79	0.68	0.62
				Fen		
2006	1828	0.40	0.91	0.71	0.83	0.72
2007	1828	0.16	0.91	0.74	0.79	0.57
2008	1828	0.17	0.99	0.79	0.71	0.61
2009	1683	0.17	0.97	0.79	0.73	0.65

[a] All measured values were recorded at $u^* > 0.2\ m\ s^{-1}$.
[b] $Y = a + bX$ from regression of simulated Y on measured X.
[c] RMSD from regression of measured Y on simulated X.
[d] Estimated from *Richardson et al.* [2006].

change in C_a or climate (baseline); (2) increasing C_a; (3) increasing C_a and T_a; and (4) increasing C_a, T_a, and precipitation to separate modeled impacts of each of these climate change factors on ecosystem productivity and PFT composition.

4. Results

4.1. Modeled Versus Measured Hourly CO_2 Fluxes

Hourly CO_2 fluxes in each landscape segment (Figure 1) were modeled as the sum of CO_2 fixation (C1–C12), less R_a (C13–C17) by all plant populations, and R_h (A11–A25) by all microbial populations. Regressions of hourly modeled CO_2 fluxes versus hourly-averaged measured CO_2 fluxes for the mixed tundra and fen sites gave intercepts within $0.2\ \mu mol\ m^{-2}\ s^{-1}$ of zero (except for the fen in 2006), and slopes within 0.1 of unity for both sites, indicating limited bias in modeled values for all years of the study (Table 2). Values for coefficients of determination (R^2) and root-mean-squares for differences between modeled and EC fluxes (RMSD) were 0.7–0.8 ($P < 0.0001$) and 0.6–$0.8\ \mu mol\ m^{-2}\ s^{-1}$, respectively (Table 2). These values were considered acceptable given the EC energy balance closure of 0.80 reported for this site [*Lafleur and Humphreys*, 2008] because the mechanisms responsible for incomplete energy balance closure have important consequences for the calculation of CO_2 fluxes measured with open-path infrared gas analyzers [*Liu et al.*, 2006; *Wilson et al.*, 2002] such as those used at Daring Lake. Much of the variance in EC fluxes unexplained by *ecosys* could be attributed to a random error of 20–30% in EC methodology for fluxes of the magnitudes measured in this study [*Kessomkiat et al.*, 2013]. This attribution was corroborated by root-mean-square error (RMSE) for EC measurements at Daring Lake calculated from the equations of *Richardson et al.* [2006] that were similar to RMSD, indicating that further constraint in model testing could not be achieved without further precision in EC measurements.

4.2. Modeled Versus Measured Seasonal and Annual Net CO_2 Exchange

4.2.1. Snowpack and Active Layer Depths

The study period included a cold year (2004), a cool year (2005), followed by a comparatively warm year (2006), a dry year (2007), a near-average year (2008), and a cool year (2009) (Table 3). Differing weather during this period caused differing seasonal profiles of ice-free zones (Figures 2a–2j) and of snowpack and ALD (Figures 3a and 3b) to be modeled in the mixed tundra and fen from 4 min solutions to the general heat flux equation (D13) driven by surface energy exchange (D11) and subsurface heat transfer (D12) in the snowpack, surface residue, and soil layers. The accuracy with which snowpack depth can be modeled is affected by the accuracy with which snowfall events can be measured and by wind-driven redistribution of snow over the landscape which was not included in the model. However, this accuracy is important to modeling dates of snowmelt (Table 3) and consequent soil thawing (Figure 3). Both modeled and

Table 3. Average Temperature, Total Precipitation, Date of Snowmelt, and Net CO_2 Exchange From Gap-Filled Eddy Covariance Measurements (EC) and Modeled Over Mixed Tundra and Fen Sites at Daring Lake From 15 May to 31 August in 2006 to 2009[a]

			Snowmelt				Net CO_2 Exchange			
			DOY				g C m^{-2}			
	Average Temperature	Precipitation	Mixed Tundra		Fen		Mixed Tundra		Fen	
Year	°C	mm	observed	modeled	observed	modeled	EC	modeled	EC	modeled
2005	6.8	114	152	149	not applicable (na)	153	50 (±0.6)	44	na	78
2006	10.3	163	130	129	130	132	62 (±0.8)	58	111 (±0.8)	108
2007	8.2	60	152	143	145	145	66 (±0.8)	67	63 (±0.7)	90
2008	9.2	184	143	141	143	143	74 (±0.8)	58	81 (±0.7)	91
2009	6.6	87	160	156	161	156	70 (±0.8)	41	68 (±0.6)	72

[a]EC data from *Humphreys and Lafleur* [2011].

measured ALDs started immediately after snowmelt, increased until mid-September, and then modeled ALD declined with freezing downward from the surface and upward from the permafrost in October–November (mixed tundra) or November–December (fen). Increases in modeled ALD were close to those measured in mixed tundra during all years of the study (Figure 3a) but were slower than those in the fen during 2007 and 2008 (Figure 3b). ALD modeled and measured at the mixed tundra was smallest during the cooler year 2005 following the cold year 2004, greatest during the warmest year 2006, intermediate during the near-average years 2007–2008, and smaller during the cooler year 2009. ALD modeled and measured at the fen was also smaller during the cooler year 2009 than during the near-average years 2007 and 2008, but interannual variation in ALD was smaller than that in the mixed tundra. Maximum ALD in the model was within the range of 0.81 ± 0.13 m in the mixed tundra and 0.63 ± 0.02 m in the fen reported by *Lafleur et al*. [2012] and close to 0.55 m measured in the fen on day of year (DOY) 240 in 2008 by *Wilson and Humphreys* [2010] (Figure 3).

4.2.2. Seasonal Net CO_2 Exchange

In the model, ALD affected net CO_2 exchange by determining the volume of soil within which T_s and θ (D13) were favorable for R_h (A11 from A4 and A6), and hence microbial nutrient mineralization (A26 from A21 and A25), root nutrient uptake (C23 from C21 and C22), and thereby CO_2 fixation (C1 from C6 and C8). At the mixed tundra site, seasonal net CO_2 uptake modeled in *ecosys* did not vary with seasonal weather or ALD during warmer years from 2006 to 2008 but declined during cooler years with later snowmelts in 2005 and 2009 (Table 3). These declines were caused by later onset of net CO_2 uptake in spring (e.g., Figure 4k in 2009 versus Figures 4b, 4e, and 4h in 2006–2008) with later snowmelt (Figure 3a) and cooler T_a (Figure 4j versus Figures 4a, 4d, and 4g). A similar decline in seasonal NEP was apparent in the EC-derived value for 2005 (Table 3). However, the later onset of net CO_2 uptake modeled in 2009 was not apparent in the EC measurements (Figure 4k). Seasonal net CO_2 uptake derived from EC measurements was found not to vary with seasonal weather by *Humphreys and Lafleur* [2011] (Table 3).

At the fen site, both modeled and measured seasonal net CO_2 uptake were greater during 2006 than during 2007–2009 due to an earlier and more rapid rise in spring uptake (Figure 4c versus Figures 4f, 4i, and 4l) with warmer spring T_a (Figure 4a versus Figures 4d, 4g, and 4j), earlier snowmelt (Table 3 and Figure 3b), and deeper ALD (Figure 2d). Lower net CO_2 uptake modeled with later snowmelt and cooler spring T_a in 2005 and 2009 was not clearly apparent in the EC-derived values (Table 3). Seasonal net CO_2 uptake in the model was greater than that derived from EC measurements (Table 3) because modeled uptake persisted into September while EC uptake terminated at the end of August (Figures 4c, 4f, 4i, and 4l).

4.2.3. Annual C Balances

Differences in seasonal net CO_2 uptake modeled in the mixed tundra versus fen (Table 3) were caused by differences in GPP, R_a, and R_h (Table 4). For all years of the study, annual GPP modeled in the fen was similar to that in the mixed tundra, but belowground R_a in the poorly drained fen was limited by O_2 constraints in saturated soil below the shallow water table (C13 and C14) so that NPP modeled in the fen was larger (Table 4). Annual R_h modeled in the fen was also limited by O_2 constraints (A14 from A17) and hence was less than, or similar to, that in the mixed tundra, except in 2007. Consequently, annual NEP

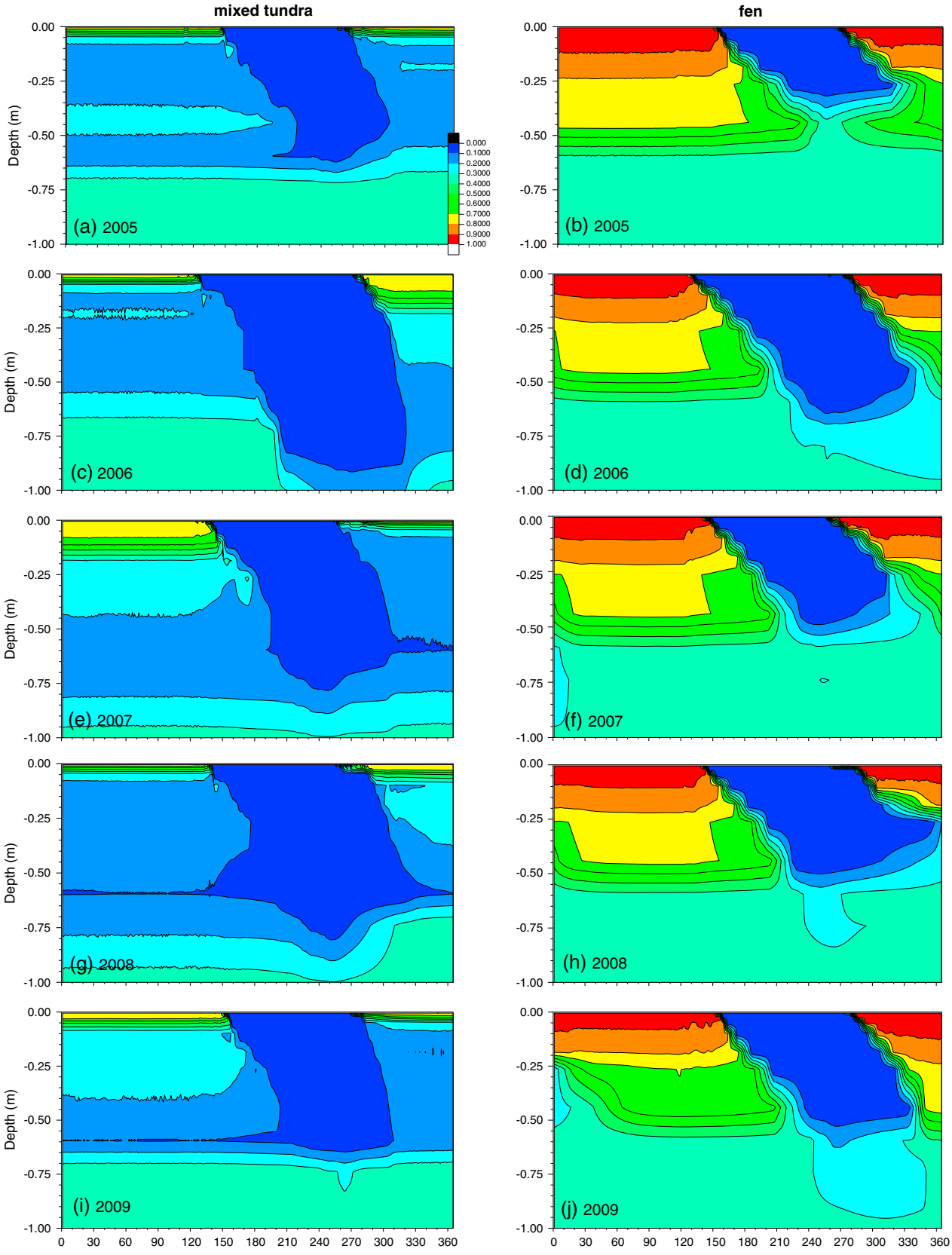

Figure 2. Ice content ($m^3\ m^{-3}$) of soil profiles modeled at the (a, c, e, g, and i) mixed tundra and (b, d, f, h, and j) fen sites from 2005 to 2009 in the transect at Daring Lake. Ice-free zones are indicated by dark blue. Smaller ice contents modeled in the mixed tundra versus fen were caused by drier and denser soil (Table 1).

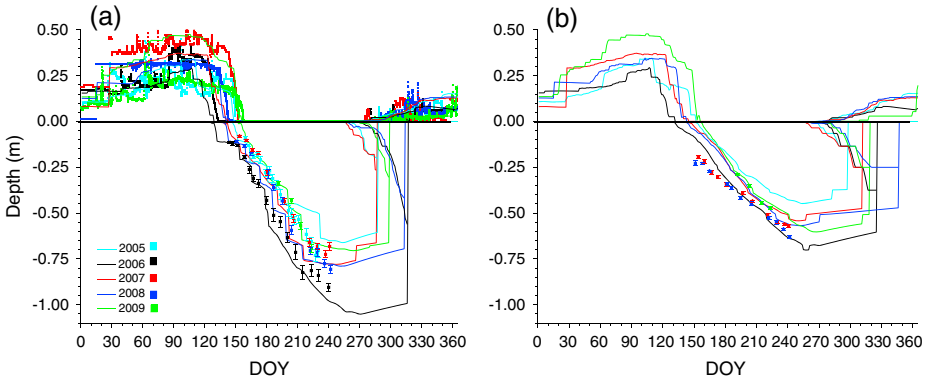

Figure 3. Depths of snowpack (positive) and depths of surface freezing and permafrost thawing (negative) modeled (lines) and measured (symbols) at (a) mixed tundra and (b) fen sites from 2005 to 2009 in the transect at Daring Lake. Continuous measurements of snowpack depth were not available for the fen.

modeled in the fen was greater than that in the mixed tundra (Table 4) as was seasonal net CO_2 exchange (Table 3). During 2007, very low precipitation in spring and early summer (Figure 4d) caused surface drying in the better drained mixed tundra which reduced R_h (A4) (Table 4) and hence raised net CO_2 uptake before rewetting in mid-July (Figures 4d and 4e). However, rewetting of the mixed tundra from

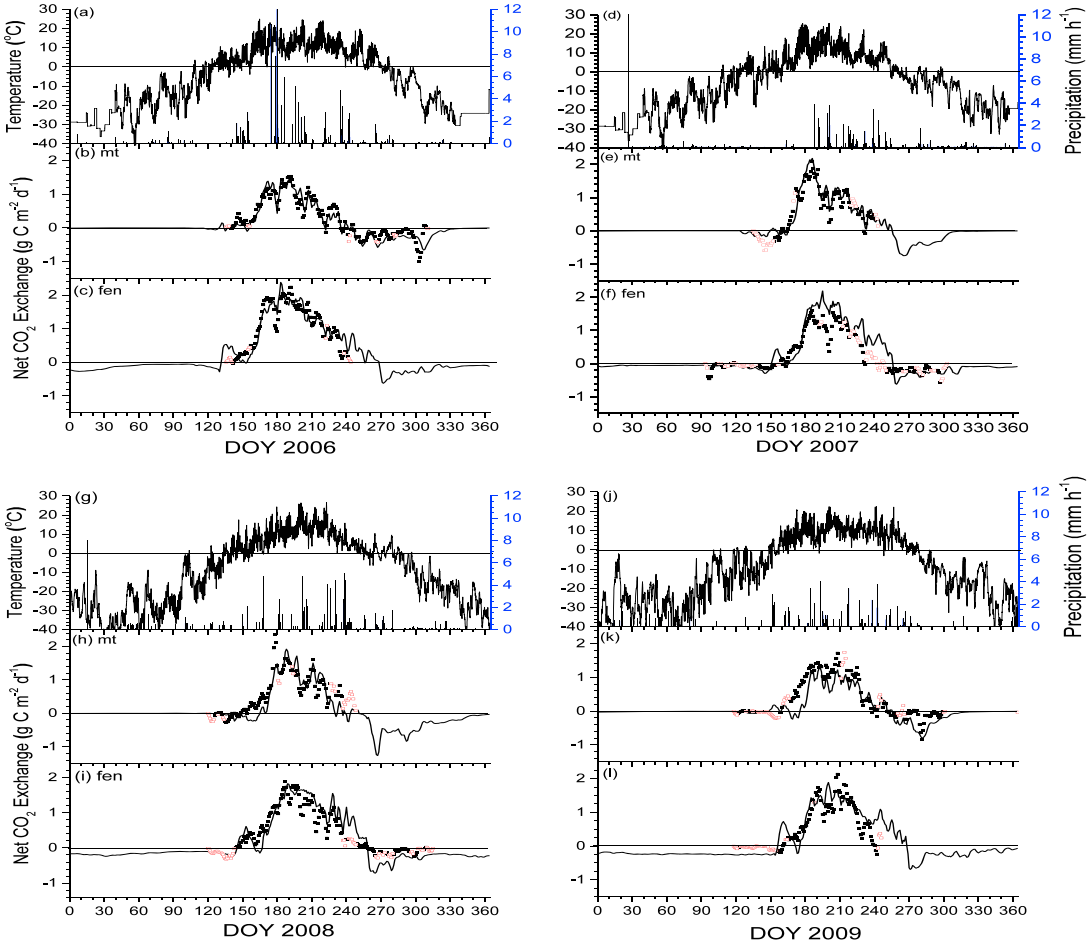

Figure 4. (a, d, g, and j) Hourly temperature and precipitation and daily net CO_2 exchange from gap-filled eddy covariance measurements (symbols) and from *ecosys* (lines) over (b, e, h, and k) mixed tundra and (c, f, i, and l) fen sites at Daring Lake from 2006 to 2009. The positive values indicate the net CO_2 uptake. The open symbols for daily net CO_2 exchange represent values consisting of more than 24.5 hourly gap-filled fluxes.

Table 4. Recorded Average Temperature, Total Precipitation, and Modeled Annual Carbon Balances For Mixed Tundra and Fen Sites at Daring Lake, NWT, From 2006 to 2009[a]

Year	2005		2006		2007		2008		2009	
Average temperature (°C)	−8.9		−6.5		−9.4		−10.2		−9.6	
Total precipitation (mm)	224		288		155		277		171	
C balance	Mixed tundra (MT)	Fen	MT	Fen	MT	Fen	MT	Fen	MT	Fen
					$g\,C\,m^{-2}\,y^{-1}$					
GPP	276	251	375	357	291	304	298	310	311	301
R_a:aboveground	−54	−71	−73	−100	−60	−89	−62	−93	−63	88
:belowground	−81	−39	−110	−46	−86	−41	−98	−43	−88	−40
NPP	140	141	191	210	154	174	138	174	161	173
R_h	−120	−88	−161	−126	−99	−123	−121	−128	−139	−139
R_e	−255	−198	−345	−272	−244	−253	−281	−264	−290	−267
Δ DIC[b]	0	3	0	0	0	2	1	2	−1	−3
NEP (CO_2)	20	56	30	85	47	53	19	48	21	34
CH_4	0	−2.3	0	−3.5	0	−2.6	0	−3.0	0	−4.8
Δ DIC, DOC[c]	0	−2	0	−3	0	−1	−1	−6	0	−5
NBP	20	52	30	78	47	50	18	39	21	24
					$g\,N\,m^{-2}\,y^{-1}$					
N_2 fixation:s[d]	0.03	0.64	0.04	0.88	0.04	0.68	0.04	0.71	0.03	0.62
:n-s	0.07	0.07	0.10	0.10	0.06	0.10	0.08	0.10	0.08	0.11
N Net Miner'n	0.62	0.16	1.01	0.32	0.65	0.22	0.70	0.31	0.87	0.26

[a]The positive values represent gains, and the negative values represent losses.
[b]Changes of dissolved inorganic C in soil.
[c]Fluxes of dissolved inorganic and organic C across external boundaries.
[d]s: symbiotic fixation in moss (fen) and lichen (mixed tundra), n-s: nonsymbiotic fixation in soil.

precipitation later in 2007 caused a sustained rise in R_h, reducing net CO_2 uptake and NEP in 2008 (Table 4 and Figures 4g and 4h).

Contrasting effects of warmer versus cooler weather on net CO_2 uptake in the mixed tundra versus fen (Table 3) were also apparent in annual C fluxes (Table 4). In the mixed tundra, warmer weather, drier soil, and hence deeper ALD during 2006 (Figures 2 and 3) raised GPP only slightly more than R_a and R_h from those modeled during cooler years with similar precipitation in 2005 and 2008, so that NEP was only slightly raised (Table 4). Increases in GPP with warming were attributed to more rapid carboxylation and respiratory kinetics, represented by the low-temperature inactivation terms in Arrhenius equations used to model the temperature dependence of CO_2 fixation (C10), R_a (C22), and R_h (A6). This term caused Q_{10} derived from these equations to rise with lower temperatures (Grant 2014), as found in experimental studies on the temperature dependence of CO_2 fixation by *Fu and Gibbs* [1987], and of R_h by *Tuomi et al.* [2008], so that sensitivity of biological reactions to temperature was greater in cooler climates. In the fen, however, warmer weather during 2006 raised GPP similarly to that in the mixed tundra but raised modeled R_e less (Table 4). This smaller rise in R_e was attributed to greater O_2 constraints (C13 and A14) and to less soil warming in wetter soil, apparent as a smaller increase in ALD (Figure 3), so that NEP modeled in the fen rose during 2006 as found experimentally by *Humphreys and Lafleur* [2011] (Table 3).

Modeled GPP was partially sustained in the mixed tundra, and more so in the fen, from biological N_2 fixation by microbial symbionts (F12–F20) (Table 4) which exchanged nonstructural N for nonstructural C and P with the lichen (mixed tundra) and moss (fen) canopies (F21–F26). Fixation rates were similar to ones of 0.14 and $1.09\,g\,N\,m^{-2}\,y^{-1}$ estimated by *Stewart et al.* [2011] from field measurements in heath-lichen tundra and wet-sedge meadow, respectively, at Daring Lake in 2007 and 2008. Modeled GPP was also sustained by nonsymbiotic N_2 fixation (A27) and N net mineralization (A25), particularly in the mixed tundra (Table 4). All these plant N sources rose with warming in the mixed tundra and the fen (2006) but declined with drying in the mixed tundra (2007).

Annual NEP in the model (Table 4) was lower than seasonal NEP (Table 3) because CO_2 exchange modeled from 1 September to 14 May each year caused net losses of C, mostly during September and October, particularly in 2008 (Figure 4). Greater annual NEP modeled in the fen versus mixed tundra was more than

offset in terms of radiative forcing by losses of CH_4 as well as of DOC from the fen (Table 4), as proposed in hypothesis 4. These losses are described in more detail in section 4.4 below.

4.3. Weather Effects on Diurnal CO_2 and Energy Exchange

4.3.1. Temperature Effects on CO_2 Uptake

Greater NEP modeled in the fen versus mixed tundra (Tables 3 and 4) was most apparent when net CO_2 uptake by the mixed tundra declined during summer warming events (e.g., Figure 4b versus Figure 4c in July 2006 and Figure 4h versus Figure 4i in July 2008). Differences in responses of uptake to T_a between the two sites were investigated by examining diurnal CO_2 and energy exchange modeled and measured during these events (Figures 5 and 6). When T_a exceeded 20°C (Figures 5a and 6a) and vapor pressure deficits (D) exceeded 1.5 kPa (Figures 5b and 6b), sharp midafternoon declines of net CO_2 uptake were modeled and measured over drier soil in the mixed tundra (DOY 201–203 in Figure 5e and DOY 199–201 in Figure 6e) but less so over wetter soil in the fen (same periods in Figures 5f and 6f). These declines indicated a more adverse effect of warming on GPP in the mixed tundra.

In *ecosys*, these declines were modeled by seeking a common value of ψ_c (B14) at which (a) root and mycorrhizal water uptake U_w (B5) driven by soil-root-canopy water potential gradients ψ_s-ψ_r-ψ_c across soil and root hydraulic resistances Ω_s and Ω_r (B9–B12) in each rooted soil layer (B6) equilibrated with (b) canopy transpiration E_c (B1) driven by vapor pressure gradients across surface resistances r_c, calculated from ψ_c in vascular plant functional types (B2), and boundary layer resistances r_a calculated from wind speeds (B3). In the mixed tundra, midafternoons with higher T_a and D caused more rapid E_c from (b) which with lower ψ_s and higher Ω_s in well-drained soil from (a) forced lower ψ_c and hence higher r_c of the vascular heath PFT that dominated the mixed tundra segments of the modeled landscape (Figure 1). These rises in r_c limited further declines in ψ_c but also limited rises in E_c and hence in latent heat LE with rises in D (Figures 5c and 6c). In the fen, midafternoons with higher T_a and D also caused more rapid E_c from (b) which also forced lower ψ_c of the nonvascular moss PFT that dominated the fen segments of the modeled landscape. However, a response of r_c to ψ_c was not modeled in nonvascular plants, so that moss r_c did not change and ψ_c was forced to decline to values at which U_w, sustained by higher ψ_s and lower Ω_s in poorly drained soil from (a), equilibrated with E_c, driven by vapor pressure gradients from the moss surface to the atmosphere from (b). Higher D thus raised E_c and LE modeled and measured in the fen (Figures 5d and 6d) as long as the surface soil remained moist.

These rises in vascular r_c caused the greater declines in midafternoon CO_2 influxes modeled in the drier mixed tundra versus the wetter fen in 2006 and 2008 (Figure 5e versus Figure 5f and Figure 6e versus Figure 6f) through coupled algorithms for CO_2 diffusion V_g (C2) and carboxylation V_c (C3) used to calculate CO_2 fixation (C1). These greater declines, corroborated by smaller LE and larger H modeled and measured under higher D in the mixed tundra than in the fen (Figure 5c versus Figure 5d and Figure 6c versus Figure 6d), support hypothesis 1 in the Introduction that net C uptake will be more adversely affected by high T_a events in mixed tundra than in fen.

4.3.2. Temperature Effects on CO_2 Emissions

Warming also affected CO_2 effluxes modeled from the mixed tundra differently than those from the fen, indicating different ecological controls on R_e. Effluxes modeled from the mixed tundra rose with warming in July 2006 to $>3\,\mu mol\,m^{-2}\,s^{-1}$ because moist surface litter and surface soil from frequent rainfall (DOY 201–203 in Figure 5b) hastened decomposition (A1) and hence microbial respiration (A11) and growth (A25) by increasing microbial habitat and hence activity (A4). CO_2 effluxes modeled from the fen during warming remained $<2\,\mu mol\,m^{-2}\,s^{-1}$ (Figure 5f) because slow aqueous O_2 diffusion through saturated soil below the water table (D16 and D19) imposed limitations to aerobic microbial (A14) and root (C14) respiration, partially offset by root O_2 uptake through aerenchyma in the sedge and birch. This slower diffusion was caused by the shallow water table maintained in the fen by downslope surface (D1) and subsurface (D9) water flow from the mixed tundra above mostly during spring melt and by lateral water exchange with the external water table (D10) through the lake boundary and lower fen (Figure 1). CO_2 effluxes measured from the mixed tundra during warming were also larger than those from the fen when the mixed tundra surface was moist in 2006 (DOY 201–203 in Figure 5e versus Figure 5f) and in 2008 (DOY 199–201 in Figure 6e versus Figure 6f), corroborating model results although comparisons were limited by

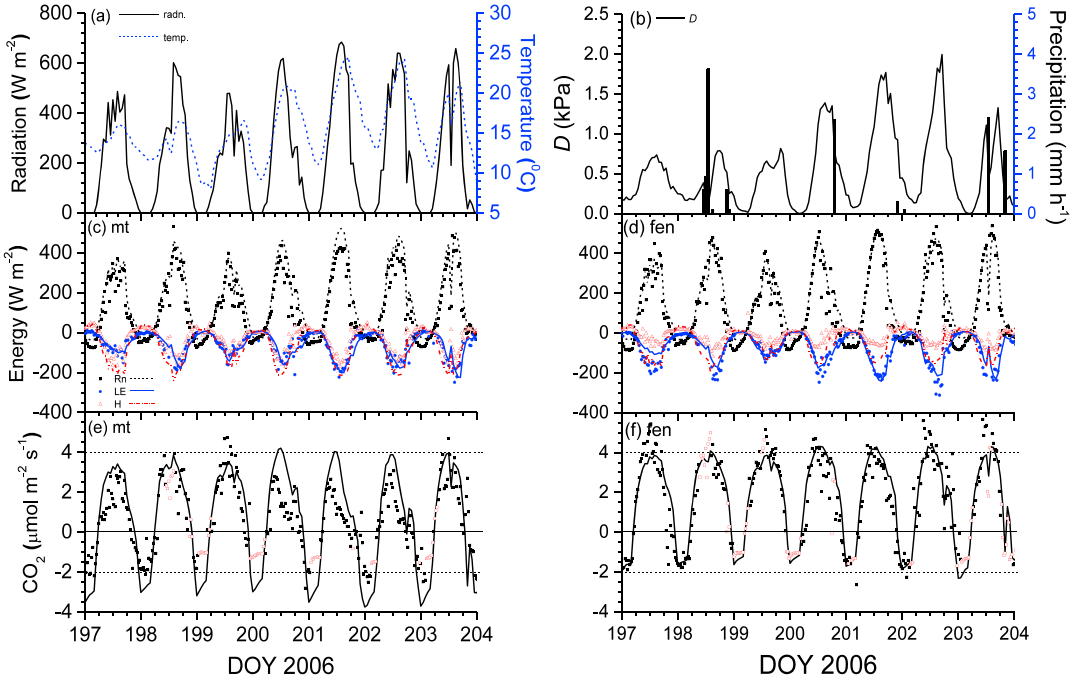

Figure 5. (a) Hourly radiation and temperature, (b) vapor pressure deficit (*D*) and precipitation, (c and d) energy, and (e and f) CO_2 fluxes measured (closed symbols) and gap-filled (open symbols) by eddy covariance and modeled by *ecosys* (lines) over (Figures 5c and 5e) mixed tundra and (Figures 5d and 5f) fen sites at Daring Lake during a warming event from DOY 198 to 204 in 2006. The positive values indicate influxes, and the negative values indicate effluxes.

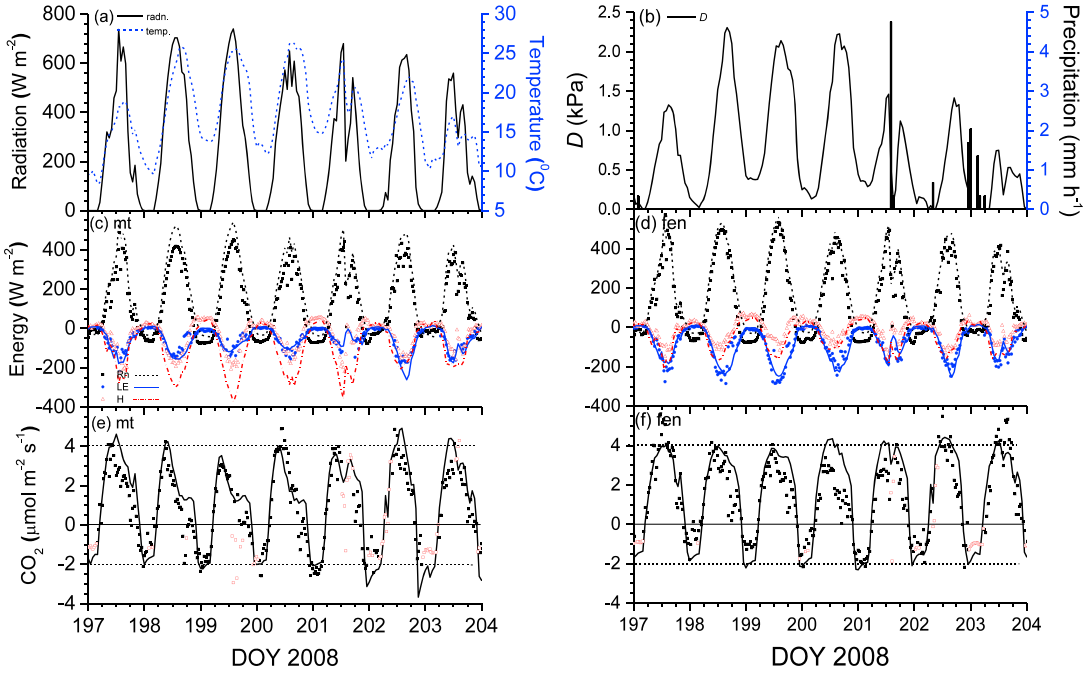

Figure 6. (a) Hourly radiation and temperature, (b) vapor pressure deficit (*D*) and precipitation, (c and d) energy, and (e and f) CO_2 fluxes measured (closed symbols) and gap-filled (open symbols) by eddy covariance and modeled by *ecosys* (lines) over (Figures 6c and 6e) mixed tundra and (Figures 6d and 6f) fen sites at Daring Lake with warming from DOY 198 to 204 in 2008. The positive values indicate influxes, and the negative values indicate effluxes.

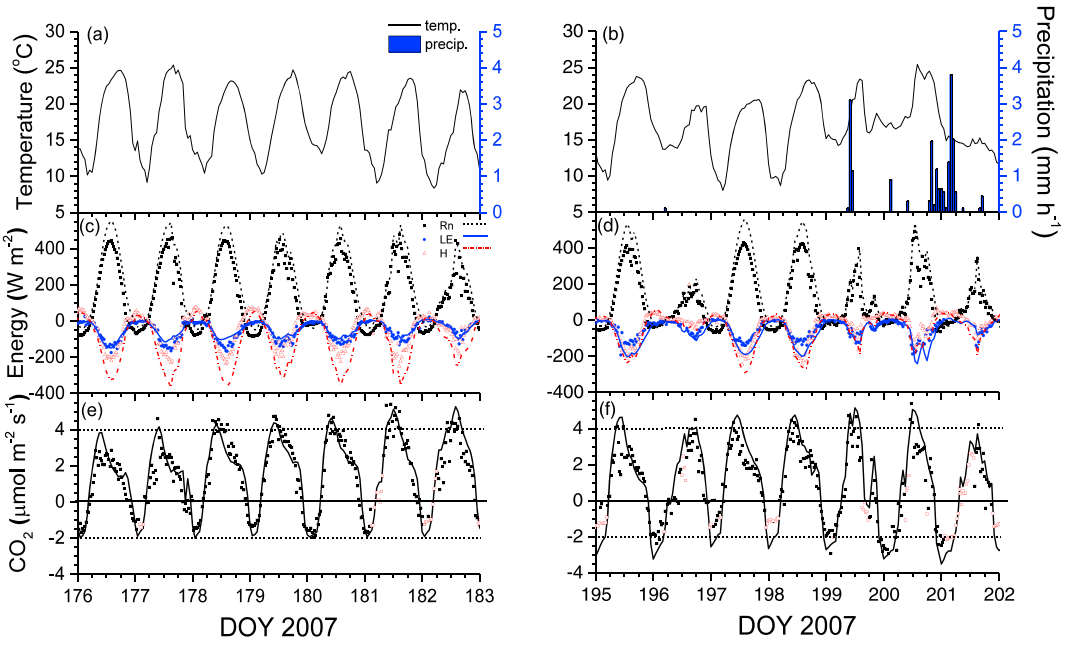

Figure 7. (a and b) Hourly temperature and precipitation, (c and d) energy, and (e and f) CO_2 fluxes measured (closed symbols) and gap-filled (open symbols) by eddy covariance and modeled by *ecosys* (lines) over mixed tundra sites at Daring Lake before wetting from DOY 177 to 183 and after wetting from DOY 196 to 202 in 2007. The positive values indicate influxes, and the negative values indicate effluxes.

the number of acceptable nighttime flux measurements. These findings support hypothesis 2 in the Introduction that R_e would rise more during high T_a events in mixed tundra than in fen. Greater daily net CO_2 uptake modeled and measured with warming in the fen versus mixed tundra in July of the wetter years 2006 (Figure 4c versus Figure 4b) and 2008 (Figure 4i versus Figure 4h) was therefore caused by both greater GPP and smaller R_e (Figure 5e versus Figure 5f and Figure 6e versus Figure 6f), consistent with hypotheses 1 and 2.

4.3.3. Precipitation Effects on Respiration

Lower and higher annual R_h were modeled in the mixed tundra during the drier and wetter years 2007 and 2008, respectively, in spite of similar mean annual temperature (MAT) (Table 4), indicating that precipitation affected R_h and hence NEP modeled in this drained upland ecosystem. The response of CO_2 exchange to precipitation in the model was investigated by examining diurnal CO_2 and energy exchange modeled and measured in the mixed tundra before and after the late onset of precipitation in 2007 (Figure 4d). CO_2 effluxes modeled and measured during DOY 177–183 before the onset of precipitation remained smaller than those modeled and measured during DOY 196–202 afterward (Figure 7e versus Figure 7f), even though T_a was higher (Figure 7a versus Figure 7b). Although R_h is not directly measured by EC, model hypotheses for the effects of θ on microbial activity and hence R_h (A4) explained the large increase in CO_2 effluxes (Figure 7) and the consequent sharp drop in NEP (Figure 4) measured by EC after the onset of precipitation in 2007.

These smaller effluxes were modeled because the surface litter and surface soil in the mixed tundra dried during periods without precipitation when surface evaporation (D6) driven by surface energy exchange (D11) exceeded upward water movement to the surface driven by water potential gradients (D7). Dry litter and surface soil were thus modeled during DOY 177–183 before precipitation, apparent in smaller *LE* and greater *H* (Figure 7c). Drying reduced CO_2 effluxes from the litter and surface soil modeled under higher T_a by slowing decomposition (A1) and hence microbial respiration (A11) and growth (A25) through reducing microbial habitat (A4) and ψ_s (A15). Subsequent wetting of litter and surface soil by precipitation increased *LE*, reduced *H* (Figure 7d), and increased CO_2 effluxes modeled during DOY 196–202 similarly to those measured (Figure 7d). CO_2 influxes modeled and measured in the mixed tundra before and after surface wetting were similar (Figure 7e versus Figure 7f), so that the late onset of precipitation in 2007 caused net

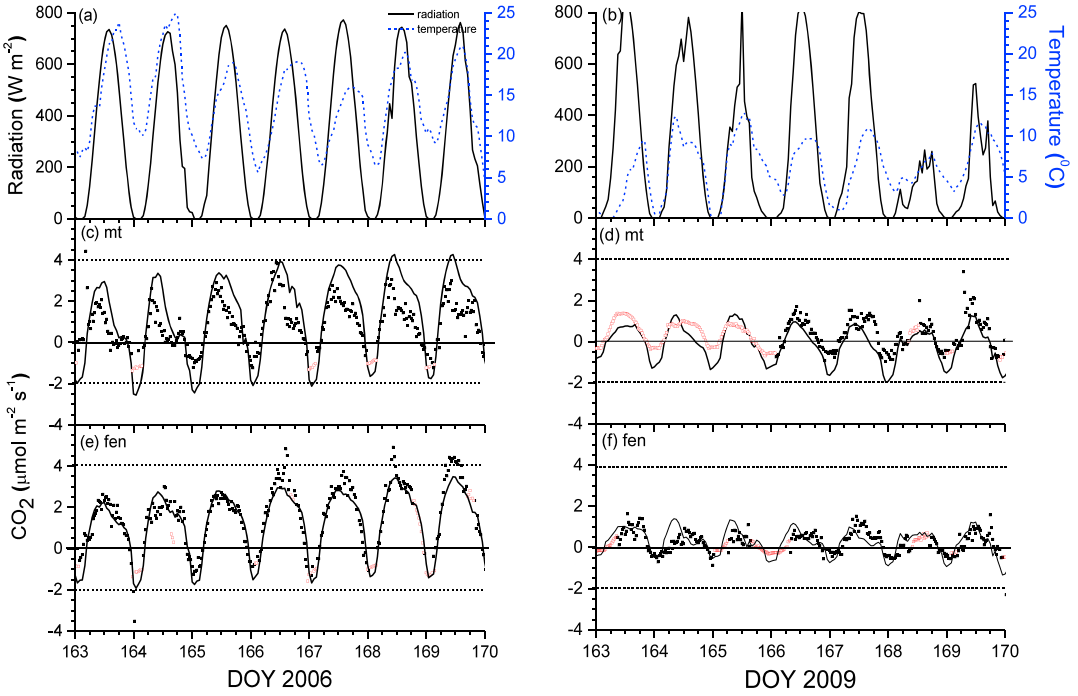

Figure 8. (a and b) Hourly radiation and temperature and (c–f) CO_2 fluxes measured (closed symbols) and gap-filled (open symbols) by eddy covariance and modeled by *ecosys* (lines) over the fen sites at Daring Lake from DOY 174 to 180 in 2006 and 2009. The positive values indicate influxes, and the negative values indicate effluxes.

CO_2 uptake to decline sharply (Figure 4e). Declines in net CO_2 uptake from increased R_h following precipitation after dry periods were also modeled and measured in the mixed tundra in 2006 (Figures 4a and 4b) and 2008 (Figures 4g and 4h). These sharp declines were neither modeled nor measured in the fen (Figures 4c, 4f, and 4i), in the model because upward water movement to the surface from the shallow water table prevented litter and surface soil from drying. Limitations on R_h imposed by surface drying caused hypothesis 2 to be refuted if warming occurred when tundra surfaces were dry.

4.3.4. Weather Effects on Net CO_2 Uptake

As shown above, CO_2 influxes declined less with rises in D, and CO_2 effluxes rose less with rises in T_a in the fen than in the mixed tundra when wet (Figures 5 and 6). Consequently, the rise in NEP with earlier snowmelt and warming was greater in the fen than in the mixed tundra (Table 4), as proposed in hypothesis 3. *Humphreys and Lafleur* [2011] attributed this greater rise to an association between earliness of net CO_2 uptake and total seasonal net CO_2 uptake in the fen that was not apparent in the mixed tundra. This association was investigated by comparing CO_2 fluxes measured and modeled following earlier snowmelt and warming in 2006 versus later snowmelt and warming in 2009 (Table 3). Larger increases in CO_2 influxes were modeled with earlier warming in 2006 versus 2009 in the wetter fen (Figure 8e versus Figure 8f) than in the drier mixed tundra (Figure 8c versus Figure 8d) where midafternoon declines occurred under higher T_a, as also occurred later in the year (Figure 5e versus Figure 5f). In *ecosys*, CO_2 fixation was modeled from prognostic, growth-driven leaf area index (LAI) (C21) that increased with earlier snowmelt and warming. CO_2 effluxes in the fen and mixed tundra increased similarly in 2006 versus 2009 but less than did CO_2 influxes. Consequently, increases in early and midseason net CO_2 uptake with earlier warming in 2006 versus 2009 were greater in the fen than in the mixed tundra (e.g., early summer NEP in the fen versus mixed tundra increased to 2.0 versus 1.4 g C m^{-2} d^{-1} in 2006 (Figure 4c versus Figure 4b) from 1.4 versus 1.2 g C m^{-2} d^{-1} in 2009 (Figure 4l versus Figure 4k)).

4.4. Diurnal and Seasonal CH_4 Emissions

4.4.1. Diurnal CH_4 Emissions

Hourly CH_4 emissions modeled from the fen were compared with surface chamber measurements taken during the summer of 2008 (Figure 9a). Modeled emissions were characterized by basal rates rising from

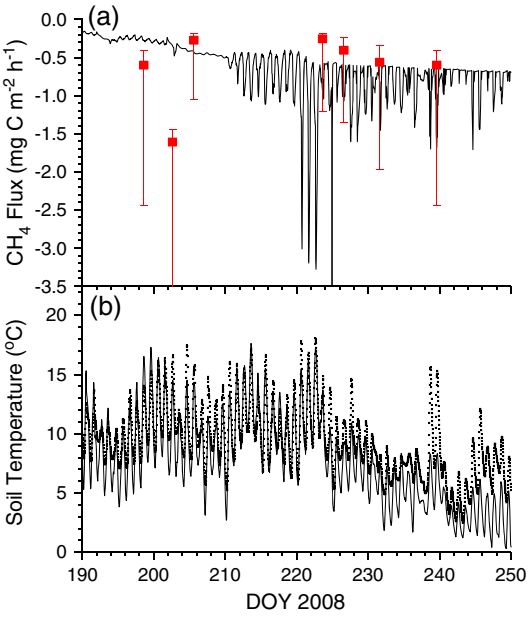

Figure 9. Hourly (a) CH_4 fluxes and (b) soil temperatures at 0.05 m measured (symbols) and modeled (line) at the fen site during summer 2008. Measured CH_4 fluxes from *Wilson and Humphreys* [2010]. The negative values indicate emissions.

0.3 to 0.6 mg C m^{-2} h^{-1}, augmented from late July to early September by diurnal increases of 1–2.5 mg C m^{-2} h^{-1} during afternoons with greater soil warming (e.g., DOY 221–224 in Figure 9b). These emissions were driven by aqueous O_2 concentrations [$O_{2(s)}$] that declined sharply with depth below the water table. In saturated soil, O_2 supply was restricted to aqueous diffusion in the soil (D19–D21) and to gaseous and aqueous diffusion through the root aerenchyma (D16–D17), causing sharp reductions in O_2 influxes in the fen versus mixed tundra (Figure 10b versus Figure 10a).

Soil warming further reduced [$O_{2(s)}$] by raising heterotrophic O_2 demand (A17 and C14). Lower [$O_{2(s)}$] slowed O_2 uptake (A17), and hence DOC oxidation, R_h (A14) and growth (A20) by aerobic heterotrophs, which slowed their assimilation of DOC products from decomposition (A21). Consequent rises in DOC concentrations drove losses of DOC from convective-dispersive solute transfer (D19) (Table 4). Lower [$O_{2(s)}$] in the model also

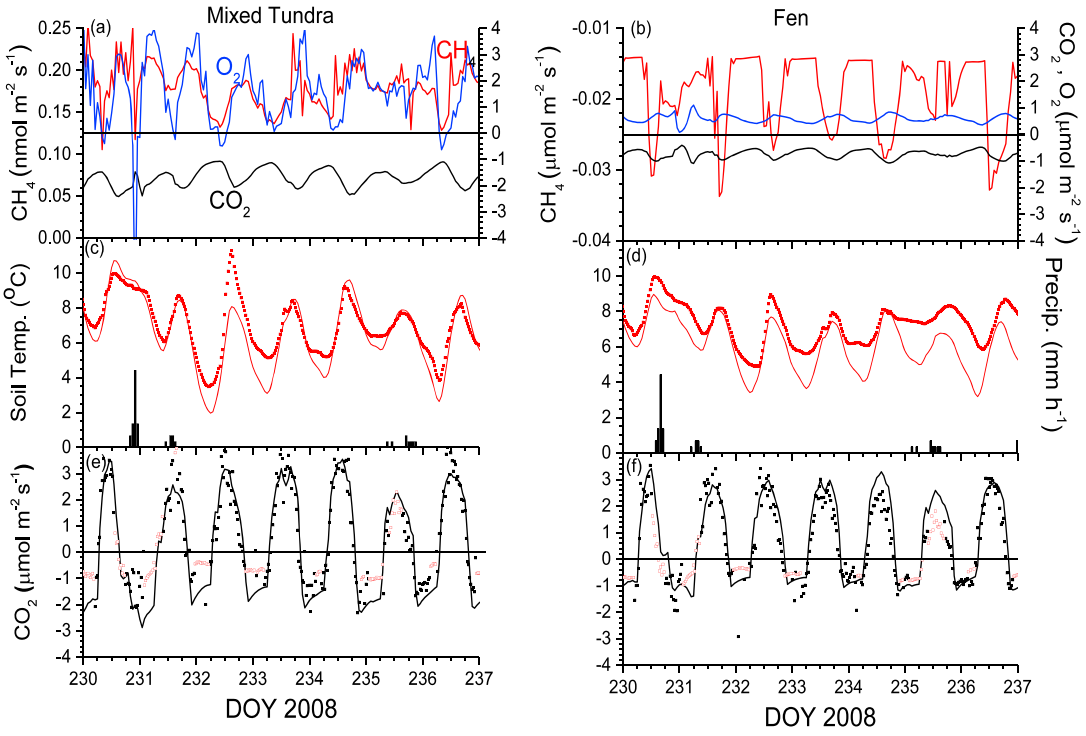

Figure 10. (a and b) Soil CH_4, O_2, and CO_2 fluxes; (b and c) soil temperatures at 0.05 m; and (e and f) ecosystem CO_2 fluxes measured (symbols) and modeled (lines) in the mixed tundra and fen sites at Daring Lake from DOY 231 to 237 in 2008. For fluxes, the positive values indicate influxes, and the negative values indicate effluxes.

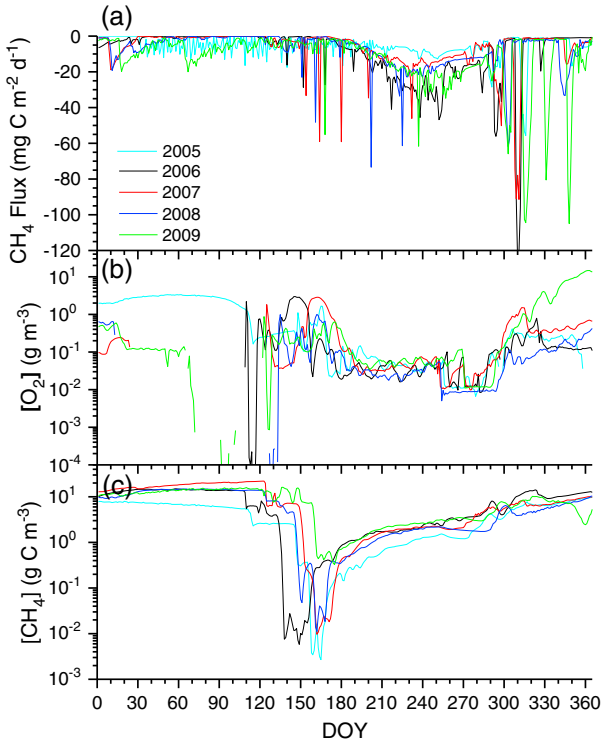

Figure 11. (a) Daily total CH_4 fluxes, (b) aqueous O_2 concentrations, and (c) aqueous CH_4 concentrations modeled 0.05 m below the soil surface at the fen site during 2005–2009. The negative fluxes indicate emissions.

alleviated O_2 constraints on oxidation, reduction (G1), and assimilation (G3) of this increased DOC by anaerobic fermenters which produced acetate and H_2 substrates for methanogenesis (G2).

The production of acetate and H_2 by fermenters drove CH_4 production from modeled heterotrophic (G7–G11) and autotrophic (G12–G17) methanogenesis, respectively. At the same time, O_2 constraints on autotrophic methanotrophy (G21) within a shallow near-surface aerobic zone limited CH_4 oxidation in the model (G18–G27). Consequent rises in aqueous CH_4 concentrations [$CH_{4(s)}$] (G8 and G14) drove bubbling (D18) and aqueous diffusion (D19) to, and volatilization (D14 and D15) from, aqueous-gaseous interfaces in soils and roots which gave the basal rates of CH_4 emission in Figure 9. The diurnal emissions (Figure 10b) were driven by degassing (D14) and bubbling (D18) of up to 2.5 mg C m^{-2} h^{-1}, mostly from 0.05 to 0.10 m below the water table, forced by declining CH_4 solubility in diurnally warming water (Figure 10d) as described in *Grant and Roulet* [2002]. However, bubbling was modeled only after total aqueous gas concentrations in the model (N_2, O_2, CO_2, CH_4, H_2, NH_3, and N_2O) reached a gaseous equivalent of one atmosphere at ambient T_a. These total concentrations remained below this value with cooler soil and slower biological activity before late July and after mid-September, during which time bubbling did not contribute to diurnal variation in modeled emissions (Figure 9a). These modeled emissions caused the annual CH_4 effluxes of 2–5 g C m^{-2} in Table 4.

The measured CH_4 emissions with which model results were compared were recorded during 2 h periods between 12:00 and 18:00 h, and so may have missed or only partly captured any late afternoon bubbling events. These measured fluxes showed large variability similar in magnitude to that of the modeled emission events (Figure 9a).

The lower energy yields of fermentation (G5) and methanogenesis (G10 and G16) from those of aerobic oxidation (A21) reduced R_h and hence CO_2 emissions modeled in the fen from those in the mixed tundra (Figure 10b versus Figure 10a). These reduced emissions were apparent in reduced ecosystem CO_2 effluxes measured and modeled in the fen versus mixed tundra (Figure 10f versus Figure 10e) and caused the reductions in annual R_h modeled in the fen during some of the years in Table 4.

In the presence of a gaseous phase in the drier mixed tundra, larger O_2 influxes (Figure 10a versus Figure 10b) maintained higher [$O_{2(s)}$], which enabled aerobic heterotrophs rapidly to oxidize DOC and aerobic autotrophs to oxidize CH_4. Oxidation reduced DOC and acetate substrates available to fermenters and methanogens, thereby reducing [$CH_{4(s)}$] and eliminating effluxes of CH_4 and DOC (Table 4), while maintaining very small influxes of CH_4 that followed those of O_2 (Figure 10a). Both measured and modeled results indicated very small net uptake of CH_4 in the mixed tundra.

4.4.2. Seasonal CH_4 Emissions

Daily-aggregated CH_4 emissions modeled from the fen during 2005–2009 remained small during winter and early spring (Figure 11a), but increased during late spring and summer with rising T_s, deepening ALD (Figure 2) and declining [$O_{2(s)}$] (Figure 11b). These increases were particularly apparent during several brief emission events

modeled during soil thawing from late May to early July, although not in all years (Figure 11a). These events occurred when surface drying following thawing opened a gaseous pathway into the soil, allowing rapid subsurface volatilization of $CH_{4(s)}$ (D14) remaining in frozen soil since the previous autumn (Figure 11c). During this period $[CH_{4(s)}]$ declined sharply from emission and dilution with soil thawing (Figure 11c).

CH_4 emissions modeled during summer were generally larger than those during spring but with less pronounced emission events (Figure 11a). Emissions modeled during summer 2005 were smaller than those modeled later because cooler weather (Table 3) caused T_s to remain low resulting in a shallower ALD (Figure 2). A large fraction (50–75%) of the modeled CH_4 effluxes was conducted to the surface through highly porous sedge roots (D14–D17), indicating that these effluxes were sensitive to modeled sedge root density. During summer, $[O_{2(s)}]$ remained low (Figure 11b) and $[CH_{4(s)}]$ rose gradually with sustained production of CH_4 (Figure 11c). The onset of large diurnal variation in CH_4 emissions in late July (Figure 9a) coincided with a rise in modeled $[CH_{4(s)}]$ above ~1 g C m^{-3} at 0.05 m, as total aqueous gas concentrations approached a gaseous equivalent of one atmosphere.

Modeled CH_4 effluxes declined with T_s during early autumn, but rose sharply with the onset of soil freezing (Figure 11a), indicated by declines in ALD caused by freezing downward from the surface and upward from the permafrost (Figures 2b, 2d, 2f, and 2h). These large effluxes were attributed in the model mostly to bubbling of $CH_{4(s)}$ (D18) at high concentrations (Figure 11c), forced by rising aqueous gas concentrations modeled with declining θ during freezing. The timing and magnitude of these autumn emission events varied greatly from year to year (Figure 11a). Modeled CH_4 effluxes declined during later autumn and winter as the depth of surface freezing moved below 0.2 m (Figure 2).

5. Discussion

5.1. Weather Effects on Net CO_2 Exchange in the Mixed Tundra

Modeled and measured net CO_2 exchange indicated that the drier mixed tundra and wetter fen at Daring Lake were net C sinks in all years of the study (Figure 4). The seasonal net CO_2 uptake modeled and measured in the mixed tundra (41–67 and 50–74 g C m^{-2}, respectively, in Table 3) was smaller than ones of 69–95 g C m^{-2} estimated from EC fluxes during eight growing seasons by *Parmentier et al.* [2011] in a mixed tussock-sedge, dwarf-shrub, and moss tundra with a continental climate at Kytalyk in NE Siberia. However, it was greater than seasonal net CO_2 uptake of −61 (C loss) to 1 g C m^{-2} estimated from EC fluxes during five growing seasons by *Kwon et al.* [2006] at a moist-tussock tundra with a continental climate but lower precipitation at Atqasuk in Alaska and of 4–40 g C m^{-2} estimated from EC fluxes during 11 growing seasons by *Lund et al.* [2012] in a high-Arctic heath tundra with a maritime climate and lower T_a at Zackenberg, Greenland.

These wide ranges of seasonal net CO_2 uptake modeled and measured across years at each of these tundra sites indicated substantial interannual variability caused by seasonal changes in weather. Seasonal net CO_2 uptake modeled at the mixed tundra site in this study fell below 50 g C m^{-2} when snowmelt was later than DOY 148 and growing seasons were cooler than 7–8°C (e.g., 2005 and 2009 in Table 3) because GPP decreased more than R_e (e.g., 2005 versus 2006 in Table 4). These declines in seasonal net CO_2 uptake were consistent with those estimated by *Grøndahl et al.* [2008] with snowmelt dates later than DOY 155 in the heath tundra at Zackenberg. The smallest net CO_2 uptake in the mixed tundra site at Daring Lake modeled with the latest snowmelt date (41 g C m^{-2} with DOY 156 in Table 3) was similar to the largest net CO_2 uptake estimated by *Lund et al.* [2012] from EC measurements at Zackenberg during the growing season with one of the earliest snowmelt dates (40 g C m^{-2} with DOY 158). This similarity indicated a continuous decline in net CO_2 uptake with later snowmelt during June for heath tundra across the two sites.

However, seasonal net CO_2 uptake modeled for the mixed tundra site at Daring Lake was not clearly associated with weather when snowmelt was earlier than DOY 149 and growing seasons were warmer than 7–8°C (e.g., 2006–2008 in Table 3). *Humphreys and Lafleur* [2011] did not find a significant correlation between snowmelt date and seasonal net CO_2 uptake derived from EC measurements for the mixed tundra site at Daring Lake. *Lund et al.* [2012] found that seasonal net CO_2 uptake declined following an unusually early snowmelt (DOY 136) at Zackenberg possibly because of water stress. *Parmentier et al.* [2011] also found no relation between seasonal net CO_2 uptake and growing season length or T_a at

Kytalyk, with similar MAT and snowmelt dates to those at Daring Lake, because R_e rose more with warming than did GPP. In *ecosys*, the limited response of net CO_2 uptake to earlier snowmelt in the mixed tundra was explained by adverse effects of warming events on CO_2 fixation over drier soil (Figure 8c versus Figure 8e).

The partial association of snowmelt date and growing season T_a with net CO_2 uptake modeled in the upland tundra at the seasonal time scale (Table 3) was less apparent at the annual time scale because greater net CO_2 uptake with warming during the growing season was offset by greater net CO_2 emission from larger litter stocks during the rest of the year (Table 4). Net emission of 17–41 g C m^{-2} modeled in the mixed tundra and of 10–25 g C m^{-2} in the fen (Table 4 versus Table 3) were similar to a total CO_2 efflux of 27 g C m^{-2} measured with surface flux chambers in a mesic birch hummock site at Daring Lake from mid-September 2004 to mid-June 2005 by *Nobrega and Grogan* [2007] but were smaller than net emissions of 66 and 33 g C m^{-2} measured with similar techniques from mesic birch hummock and wet-sedge sites, respectively, at Daring Lake from late August 2006 to mid-June 2007 by *Grogan* [2012]. These net emissions outside the growing season indicate the importance modeling and measuring full-year CO_2 exchange accounting when calculating arctic C balances.

Reduced GPP from lower g_c modeled and measured during warming events in the drier mixed tundra following earlier snowmelt in 2006 (Figure 5e) and 2008 (Figure 6e) were consistent with measured constraints on GPP imposed by higher T_a which were attributed by *Lund et al*. [2012] to reduced g_c under higher D in a high-Arctic tundra heath at Zackenberg. These constraints would be greater at sites with continental climates such as Kytalyk where intense warming events occur, possibly causing the declines in GPP during warmer growing seasons found by *Parmentier et al*. [2011]. However modeled R_e continued to rise sharply with warming at these sites from high Q_{10} in cold soils, adversely affecting net CO_2 exchange as has also been found with experimental warming. Artificial warming of 9°C was found to raise R_e more than CO_2 fixation at a tundra site near Zackenberg by *Marchand et al*. [2005], which was consistent with more rapid net C loss under higher T_a and D measured by *Kwon et al*. [2006] in the moist-tussock tundra at Atqasuk. Such losses reduced the response of net CO_2 uptake to earlier snowmelt in warmer years in tundra with continental climates.

Wetting of litter and surface soil from precipitation was found to increase R_h and hence R_e modeled in the mixed tundra (Figure 7), causing short-term reductions in NEP (e.g., 2008 versus 2007 in Table 4). However, increased R_h also drove more rapid N net mineralization in rewetted litter and surface soil (A25) which sustained greater GPP thereafter (Table 4). The larger CO_2 effluxes modeled with rewetting (Figure 7) were consistent with pulses of CO_2 effluxes commonly observed after rewetting of previously dry soil surfaces [*Huxman et al*., 2004] as modeled by *ecosys* elsewhere [*Grant et al*., 2012a]. Similar increases in tundra CO_2 emissions have been measured after experimental wetting of tundra soil, so that increases in precipitation widely projected for arctic regions are expected to have important effects on tundra C balances [*Christiansen et al*., 2012; *Lupascu et al*., 2014; *Sharp et al*., 2013].

5.2. Weather Effects on Net CO_2 Exchange in the Fen

The net CO_2 uptake modeled and measured during the four growing seasons in the fen (72–108 g C m^{-2} in Table 3) were similar to ones of 50–123 g C m^{-2} estimated from EC fluxes by *Rennermalm et al*. [2005] during five growing seasons in a fen with a maritime climate at Zackenberg, Greenland, with an ALD similar to that at the fen in this study. This uptake was smaller than ones of 104–161 g C m^{-2} estimated by *Harazono et al*. [2003] during two growing seasons, but larger than ones of 49–70 g C m^{-2} estimated by *Kwon et al*. [2006] during five growing seasons, from EC fluxes at coastal wet-sedge tundras with a maritime climate near Barrow, Alaska, with lower T_a and a shallower ALD. This uptake was also larger than one of 59–69 g C m^{-2} estimated by *Humphreys et al*. [2014] over two growing seasons at two bogs in northern Ontario near the southern limit of permafrost and of 4–53 g C m^{-2} estimated by *Aurela et al*. [2004] in a mesotrophic fen at Kaamanen in northern Finland. Net CO_2 uptake in arctic wetlands is thus consistently greater than that in uplands, due in part to symbiotic N_2 fixation in moss [*Stewart et al*., 2011] (Table 4).

Seasonal net CO_2 uptake modeled and measured in the wetter fen responded differently to changes in weather than did that in the drier mixed tundra. Earlier snowmelt and a warmer growing season increased net CO_2 uptake in the fen (e.g., 2006 versus 2009 in Table 3) by hastening early LAI growth and thereby

raising GPP more than R_e (Figure 8e versus Figure 8f) to a greater extent than in the mixed tundra (Figure 8c versus Figure 8d). This response to earlier snowmelt appears to occur widely in Arctic fens and other wetlands. *Aurela et al*. [2004] found a gain of 2.0 g C m^{-2} y^{-1} in the annual CO_2 balance at a fen at Kaamanen, Finland, for each 1 day advance in the snowmelt date, somewhat larger than the gain of 1.5 g C m^{-2} y^{-1} d^{-1} modeled for the fen at Daring Lake (Tables 3 and 4). *Kwon et al*. [2006] attributed rapid early-season C gain in a wet-sedge tundra at Barrow, Alaska, to greater photosynthetic capacity due to early onset of plant development with earlier snowmelt and to slow R_e from low T_s in frozen soils. *Rennermalm et al*. [2005] attributed greater seasonal net CO_2 uptake in a high-Arctic fen at Zackenberg to earlier LAI growth enabled by earlier snowmelt. *Griffis et al*. [2000] also attributed greater net CO_2 uptake by a fen in sub-Arctic Manitoba to early snowmelt combined with wet and warm weather during spring. Interannual variability in net CO_2 exchange has been found to be determined more by GPP and less by R_e in Arctic fens than in mesic and dry upland Arctic tundra [*Griffis et al*., 2000; *Kwon et al*., 2006], as modeled here (Table 4 and Figure 8).

5.3. Weather Effects on CH_4 Emissions in the Fen

Annual CH_4 emissions modeled from the fen at Daring Lake varied from 2.3 to 4.8 g C m^{-2} (Table 4), similar to ones estimated from EC fluxes of 3.15 g C m^{-2} by *Wille et al*. [2008] over a wet tundra with a continental climate on Samoylov Island in Siberia, and ones of 2.8 ± 0.4 g C m^{-2} (June–August) and 6.5–7.9 g C m^{-2} (June–October) by *Friborg et al*. [2000] and *Tagesson et al*. [2012], respectively, over a high-Arctic fen with a maritime climate at Zackenberg, Greenland. However, the annual modeled emissions were smaller than ones estimated from EC fluxes of 15–17 g C m^{-2} by *Jackowicz-Korczyński et al*. [2010] over the graminoid section of the warmer Stordalen subarctic palsa mire in Sweden. The increase in CH_4 emissions modeled from 2005 to 2006 with increasing GPP (Table 4), T_s, and ALD (Figure 2) and the subsequent decline in CH_4 emissions modeled from 2006 to 2007 and 2008 with decreasing GPP, T_s, and ALD (Table 4 and Figure 11a) were consistent with the findings of *Tagesson et al*. [2012] that total growing season CH_4 fluxes were well correlated with GPP, T_s, and ALD.

However, the large and complex diurnal variation in modeled fluxes (Figures 9a and 11a) precluded any simple associations with θ, T_s, and ALD. Much of this variation was driven by physical processes controlling gas transfers and release in the model, such as volatilization and diffusion, the parameterizations of which were well constrained from basic properties of gases such as solubility and diffusivity. While total aqueous gas concentrations remained below a gaseous equivalent of one atmosphere, these processes caused diurnal variation in modeled fluxes to remain very small (Figure 9a). However, once total aqueous gas concentrations reached this gaseous equivalent, these same processes forced degassing with diurnal soil warming (e.g., Figure 9a), greatly increasing the sensitivity of CH_4 emissions to T_s. This increased sensitivity enabled the large apparent Q_{10} values frequently fitted to experimental studies [e.g., *Walter and Heimann*, 2000] to be modeled with biologically realistic Q_{10} values ((A6); see Figure 2 in *Grant* [2015]). The model thus simulated both the absence of diurnal variation in CH_4 emissions found in some studies [*Jackowicz-Korczyński et al*., 2010; *Tagesson et al*., 2012] and the large diurnal variation found during the warmer part of the growing season in other studies [*Friborg et al*., 2000; *Long et al*., 2012; *Nakano et al*., 2000].These same well-constrained processes controlling gas transfers and release in the model also drove several emission events during soil thawing in spring and freezing in autumn (Figure 11a). In spring, these events were caused by the reestablishment of gaseous pathways through the near-surface soil to the atmosphere with thawing (Figure 2) that hastened volatilization of aqueous CH_4 stored in unfrozen water over the previous winter. In autumn these events were caused by declining θ during freezing (Figure 2) that forced volatilization of much of the aqueous CH_4 remaining from the previous summer. The simulated CH_4 emission events were thus an intrinsic model response to soil thawing and freezing, the timing and rates of which varied greatly from year to year. Corresponding CO_2 emission events were also modeled, but these were much smaller than those of CH_4 relative to annual emissions.

These emission events were sustained by high [$CH_{4(s)}$] modeled during spring and autumn that had risen gradually from lower values modeled during summers (Figure 11c). These summer [$CH_{4(s)}$] were similar to concentrations of 0.5–1.5 g C m^{-3} recorded in a subarctic wetland in northern Sweden, over which CH_4 emissions of 1–6 mg C m^{-2} h^{-1} were measured by *Ström and Christensen* [2007], and to concentrations

of 1.2–3.6 g C m^{-3} recorded at a subarctic tundra in western Siberia, over which CH_4 emissions of 0.25–7.5 mg C m^{-2} h^{-1} were measured by *Heyer et al*. [2002]. This similarity of measured and modeled CH_4 concentrations (Figure 11c) and emissions (Figure 11a) during summer indicated that physical processes governing CH_4 transfers and release were likely to have been accurately modeled. However, measurements to corroborate larger [$CH_{4(s)}$] modeled during spring and autumn emissions are lacking, likely because water extraction from partially frozen soil would be difficult.

Emission events similar to those modeled during spring and autumn (Figure 11a) have frequently been reported from field studies. *Friborg et al*. [1997] measured rapid rises in CH_4 emissions during spring thaw in a subarctic mire which they attributed to release of subsurface CH_4 accumulated during winter. *Heyer et al*. [2002] sometimes measured greater CH_4 emissions, with greater temporal variation, in spring than in summer at a subarctic tundra in western Siberia, even when air temperatures were 10°C lower. Sudden increases in emissions to ~5 mg C m^{-2} h^{-1} measured in spring were associated with drops in water table during thawing, rather than with soil warming [*Heyer et al*., 2002]. Most of these emissions were attributed to CH_4 generated the previous year, as modeled in this study (Figure 11a).

The large-emission events modeled during soil freezing in late October and November (Figure 11a) were consistent with a large CH_4 emission events of up to 300 mg C m^{-2} d^{-1} measured during soil freezing in autumn by *Mastepanov et al*. [2008] with automated chambers in the high-Arctic fen at Zackenberg. This measured burst was attributed by *Mastepanov et al*. [2008] to degassing during freezing, as were the emission events in this study. *Sturtevant et al*. [2012] reported brief CH_4 emission events of up to 72 mg C m^{-2} d^{-1}during autumn freezing from EC and chamber flux measurements on a wet-sedge tundra near Barrow, Alaska. These events were associated with high wind speed, which can induce bubbling. Autumn CH_4 emissions in the model contributed 0.3–0.4 of annual CH_4 emissions. This contribution was larger than one of 0.21–0.25 estimated by *Sturtevant et al*. [2012] from EC fluxes but was similar to one of 0.35 estimated by *Wille et al*. [2008] from EC fluxes over a wet tundra on Samoylov Island in Siberia. Autumn CH_4 emissions are thus an important component of annual CH_4 emissions used in greenhouse gas inventories, so that the degassing processes thought to drive these emissions need to be represented in models used to estimate these inventories. However, large interannual variation in the timing and magnitude of both spring and autumn emission events in the model (Figure 11a) would require extended, continuous measurements of early and late season emissions to be corroborated.

5.4. Implications for Effects of Long-Term Climate Warming on Net CO_2 and CH_4 Exchange

The responses to changes in seasonal weather of net CO_2 exchange in mixed tundra and fen, and of CH_4 emissions in the fen, modeled and measured in this study may have important implications for their responses to long-term climate warming. These responses suggest that fens may be better placed to increase net CO_2 uptake with climate warming than are upland tundras. However, the effects of long-term climate warming are also affected by other processes that occur at longer time scales than that of this study, notably changes in PFTs, landscape hydrology, and nutrient cycling, which may not have been fully accounted for in the short-term results presented here. Accurately modeling responses of CO_2 and CH_4 exchange to changes in seasonal weather, as attempted in this study, is a vital prerequisite to accurately modeling these responses to climate change. However, modeling these longer-term responses should also account for the longer-term processes by which these responses are also affected. These effects are best modeled by gradually incrementing meteorological boundary conditions according to climate change projections over decadal to centennial time scales, as presented in an accompanying study [*Grant*, 2015].

Acknowledgments
Computational facilities for *ecosys* were provided by the University of Alberta and by the Compute Canada high-performance computing infrastructure. A PC version of *ecosys* with GUI can be obtained by contacting the corresponding author at rgrant@ualberta.ca. The measured flux data were supported by NSERC discovery grants to P.M.L. and E.R.H. The modelling work was conducted as part of the Arctic Development and Adaptation to Permafrost in Transition (ADAPT) project funded by an NSERC Discovery Frontiers Grant.

References

Aurela, M., T. Laurila, and J.-P. Tuovinen (2004), The timing of snow melt controls the annual CO_2 balance in a subarctic fen, *Geophys. Res. Lett.*, *31*, L16119, doi:10.1029/2004GL020315.

Boelter, D. H. (1969), Physical properties of peats as related to degree of decomposition, *Soil Sci. Soc. Am. Proc.*, *33*(4), 606–609.

Christiansen, C. T., S. H. Svendsen, N. M. Schmidt, and A. Michelsen (2012), High arctic heath soil respiration and biogeochemical dynamics during summer and autumn freeze-in—Effects of long-term enhanced water and nutrient supply, *Global Change Biol.*, *18*, 3224–3236.

Dimitrov, D. D., R. F. Grant, P. M. LaFleur, and E. Humphreys (2011), Modelling the effects of hydrology on gross primary productivity and net ecosystem productivity at Mer Bleue bog, *J. Geophys. Res.*, *116*, G04010, doi:10.1029/2010JG001586.

Dimitrov, D. D., J. S. Bhatti, and R. F. Grant (2014), The transition zones (ecotone) between boreal forests and peatlands: Ecological controls on ecosystem productivity along a transition zone between upland black spruce forest and a poor forested fen in central Saskatchewan, *Ecol. Model.*, *291*, 96–108.

Elmendorf, S. C., et al. (2012), Global assessment of experimental climate warming on tundra vegetation: Heterogeneity over space and time, *Ecol. Lett.*, *15*, 164–175.
Environment Canada (2004), *2004 Canadian Acid Deposition Science Assessment*, Meteorological Service of Canada, Ottawa, Canada.
Friborg, T., T. R. Christensen, and H. Soegaard (1997), Rapid response of greenhouse gas emission to early spring thaw in a subarctic mire as shown by micrometeorological techniques, *Geophys. Res. Lett.*, *24*, 3061–3064, doi:10.1029/97GL03024.
Friborg, T., T. R. Christensen, B. U. Hansen, C. Nordstroem, and H. Soegaard (2000), Trace gas exchange in a high-Arctic valley 2. Landscape CH_4 fluxes measured and modeled using eddy correlation data, *Global Biogeochem. Cycles*, *14*, 715–724, doi:10.1029/1999GB001136.
Fu, C. F., and M. Gibbs (1987), CO_2 photoassimilation by the spinach chloroplast at low temperature, *Plant Physiol.*, *83*, 849–855.
Grant, R. F. (1998), Simulation of methanogenesis in the mathematical model *ecosys*, *Soil Biol. Biochem.*, *30*, 883–896.
Grant, R. F. (1999), Simulation of methanotrophy in the mathematical model *ecosys*, *Soil Biol. Biochem.*, *31*, 287–297.
Grant, R. F. (2015), Ecosystem CO_2 and CH_4 exchange in a mixed tundra and a fen within a hydrologically diverse Arctic landscape: 2. Modeled impacts of climate change, *J. Geophys. Res. Biosci.*, *120*, 1388–1406, doi:10.1002/2014JG002889.
Grant, R. F., and L. B. Flanagan (2007), Modeling stomatal and nonstomatal effects of water deficits on CO_2 fixation in a semiarid grassland, *J. Geophys. Res.*, *112*, G03011, doi:10.1029/2006JG000302.
Grant, R. F., and E. Pattey (2008), Temperature sensitivity of N_2O emissions from fertilized agricultural soils: Mathematical modelling in *ecosys*, *Global Biogeochem. Cycles*, *22*, GB4019, doi:10.1029/2008GB003273.
Grant, R. F., and N. T. Roulet (2002), Methane efflux form boreal wetlands: Theory and testing of the ecosystem model *ecosys* with chamber and tower flux measurements, *Global Biogeochem. Cycles*, *16*(4), 1054, doi:10.1029/2001GB001702.
Grant, R. F., W. C. Oechel, C. L. Ping, and H. Kwon (2003), Carbon balance of coastal Arctic tundra under changing climate, *Global Change Biol.*, *9*, 16–36.
Grant, R. F., T. J. Arkebauer, A. Dobermann, K. G. Hubbard, T. T. Schimelfenig, A. E. Suyker, S. B. Verma, and D. T. Walters (2007a), Net biome productivity of irrigated and rainfed maize-soybean rotations: Modelling vs. measurements, *Agron. J.*, *99*, 1404–1423.
Grant, R. F., et al. (2007b), Net ecosystem productivity of boreal jack pine stands regenerating from clearcutting under current and future climates, *Global Change Biol.*, *13*, 1423–1440.
Grant, R. F., T. A. Black, E. R. Humphreys, and K. Morgenstern (2007c), Changes in net ecosystem productivity with forest age following clearcutting of a coastal Douglas fir forest: Testing a mathematical model with eddy covariance measurements along a forest chrono-sequence, *Tree Physiol.*, *27*, 115–131.
Grant, R. F., A. G. Barr, T. A. Black, H. A. Margolis, A. L. Dunn, J. Metsaranta, S. Wang, J. H. McCaughey, and C. P.-A. Bourque (2009a), Interannual variation in net ecosystem productivity of Canadian forests as affected by regional weather patterns—A Fluxnet-Canada synthesis, *Agric. For. Meteorol.*, *149*, 2022–2039.
Grant, R. F., L. R. Hutyra, R. C. de Oliveira, J. W. Munger, S. R. Saleska, and S. C. Wofsy (2009b), Modelling the carbon balance of Amazonian rainforests: Resolving ecological controls on net ecosystem productivity, *Ecol. Appl.*, *79*(3), 445–4638.
Grant, R. F., H. A. Margolis, A. G. Barr, T. A. Black, A. L. Dunn, P. Y. Bernier, and O. Bergeron (2009c), Changes in net ecosystem productivity of boreal black spruce stands in response to changes in temperature at diurnal and seasonal time scales, *Tree Physiol.*, *29*, 1–17.
Grant, R. F., A. G. Barr, T. A. Black, H. A. Margolis, J. H. McCaughey, and J. A. Trofymow (2010), Net ecosystem productivity of temperate and boreal forests after clearcutting—A Fluxnet-Canada synthesis, *Tellus B*, *62B*, 475–496.
Grant, R. F., E. R. Humphreys, P. M. Lafleur, and D. D. Dimitrov (2011a), Ecological controls on net ecosystem productivity of a mesic Arctic tundra under current and future climates, *J. Geophys. Res.*, *116*, G01031, doi:10.1029/2010JG001555.
Grant, R. F., B. A. Kimball, M. M. Conley, J. W. White, G. W. Wall, and M. J. Ottman (2011b), Controlled warming effects on wheat growth and yield: Field measurements and modeling, *Agron. J.*, *103*, 1742–1754.
Grant, R. F., D. D. Baldocchi, and S. Ma (2012a), Ecological controls on net ecosystem productivity of a Mediterranean grassland under current and future climates, *Agric. For Meteorol.*, *152*, 189–200.
Grant, R. F., A. Desai, and B. Sulman (2012b), Modelling contrasting responses of wetland productivity to changes in water table depth, *Biogeosciences*, *9*, 4215–4231.
Griffis, T. J., W. R. Rouse, and J. M. Waddington (2000), Interannual variability of net ecosystem CO_2 exchange at a subarctic fen, *Global Biogeochem. Cycle*, *144*, 1109–1121.
Grogan, P. (2012), Cold season respiration across a low Arctic landscape: The influence of vegetation type, snow depth, and interannual climatic variation, *Artic. Antarct. Alp. Res.*, *44*(4), 446–456.
Grøndahl, L., T. Friborg, T. R. Christensen, A. Ekberg, B. Elberling, L. Illeris, C. Nordstrøm, A. Rennermalm, C. Sigsgaard, and H. Søgaard (2008), Spatial and inter-annual variability of trace gas fluxes in a heterogeneous high-Arctic landscape, *Adv. Ecol. Res.*, *40*, 473–498.
Harazono, Y., M. Mano, A. Miyata, R. C. Zulueta, and W. C. Oechel (2003), Inter-annual carbon dioxide uptake of a wet sedge tundra ecosystem in the Arctic, *Tellus*, *55B*, 215–231.
Heyer, J., U. Berger, I. L. Kuzin, and O. N. Yakovlev (2002), Methane emissions from different ecosystem structures of the subarctic tundra in Western Siberia during midsummer and during the thawing period, *Tellus*, *54B*, 231–249.
Hodkinson, I. D., N. R. Webb, J. S. Bale, and W. Block (1999), Hydrology, water availability and tundra ecosystem function in a changing climate: The need for a closer integration of ideas?, *Global Change Biol.*, *5*, 359–369.
Humphreys, E. R., and P. M. Lafleur (2011), Does earlier snowmelt lead to greater CO_2 sequestration in two low Arctic tundra ecosystems?, *Geophys. Res. Lett.*, *38*, L09703, doi:10.1029/2011GL047339.
Humphreys, E. R., C. Charron, M. Brown, and R. Jones (2014), Two bogs in the Canadian Hudson Bay Lowlands and a temperate bog reveal similar annual net ecosystem exchange of CO_2, *Arctic. Antarct. Alp. Res.*, *46*, 103–113.
Huxman, T. E., K. A. Snyder, D. Tissue, A. J. Leffler, K. Ogle, W. T. Pockman, D. R. Sandquist, D. L. Potts, and S. Schwinning (2004), Precipitation pulses and carbon fluxes in semiarid and arid ecosystems, *Oecologia*, *141*, 254–268.
Jackowicz-Korczyński, M., T. R. Christensen, K. Bäckstrand, P. Crill, T. Friborg, M. Mastepanov, and L. Ström (2010), Annual cycle of methane emission from a subarctic peatland, *J. Geophys. Res.*, *115*, G02009, doi:10.1029/2008JG000913.
Kessomkiat, W., H.-J. H. Franssen, A. Graf, and H. Vereecken (2013), Estimating random errors of eddy covariance data: An extended two-tower approach, *Agric. For. Meteorol.*, *171–172*, 203–219.
Kwon, H.-J., W. C. Oechel, R. C. Zulueta, and S. J. Hastings (2006), Effects of climate variability on carbon sequestration among adjacent wet sedge tundra and moist tussock tundra ecosystems, *J. Geophys. Res.*, *111*, G03014, doi:10.1029/2005JG000036.
Lafleur, P. M., and E. R. Humphreys (2008), Spring warming and carbon dioxide exchange over low Arctic tundra, *Global Change Biol.*, *14*, 740–756.
Lafleur, P. M., E. R. Humphreys, V. L. St. Louis, M. C. Myklebust, T. Papakyriakou, L. Poissant, J. D. Barker, M. Pilote, and K. A. Swystun (2012), Variation in peak growing season net ecosystem production across the Canadian Arctic, *Environ. Sci. Technol.*, *46*, 7971–7977.

Liu, H., J. T. Randerson, J. Lindfors, W. J. Massman, and T. Foken (2006), Consequences of incomplete surface energy balance closure for CO_2; Fluxes from open-path CO_2, H_2O infrared gas analysers, *Boundary Layer Meteorol.*, *120*, 65–85.

Long, K. D., L. B. Flanagan, and T. Cai (2012), Diurnal and seasonal variation in methane emissions in a northern Canadian peatland measured by eddy covariance, *Global Change Biol.*, *16*, 2420–2435.

Lund, M., J. M. Falk, T. Friborg, H. N. Mbufong, C. Sigsgaard, H. Soegaard, and M. P. Tamstorf (2012), Trends in CO_2 exchange in a high Arctic tundra heath, 2000–2010, *J. Geophys. Res.*, *117*, G02001, doi:10.1029/2011JG001901.

Lupascu, M., J. M. Welker, U. Seibt, X. Xu, I. Velicogna, D. S. Lindsey, and C. I. Czimczik (2014), The amount and timing of precipitation control the magnitude, seasonality and sources (^{14}C) of ecosystem respiration in a polar semi-desert, northwestern Greenland, *Biogeosciences*, *11*, 4289–4304.

Marchand, F. L., S. Mertens, F. Kockelbergh, L. Beyens, and I. Nijs (2005), Performance of high Arctic tundra plants improved during but deteriorated after exposure to a simulated extreme temperature event, *Global Change Biol.*, *11*, 2078–2089, doi:10.1111/j.1365-2486.2005.01046.x.

Mastepanov, M., C. Sigsgaard, E. J. Dlugokencky, S. Houweling, L. Strom, M. P. Tamstorf, and T. R. Christensen (2008), Large tundra methane burst during onset of freezing, *Nature*, *456*, 628–658, doi:10.1038/nature07464.

McGuire, A. D., et al. (2012), An assessment of the carbon balance of Arctic tundra: Comparisons among observations, process models, and atmospheric inversions, *Biogeosciences*, *9*, 3185–3204.

Mezbahuddin, M., R. F. Grant, and T. Hirano (2014), Modelling effects of seasonal variation in water table depth on net ecosystem CO_2 exchange of a tropical peatland, *Biogeosciences*, *11*, 577–599.

Miller, P. A., and B. Smith (2012), Modelling tundra vegetation response to recent Arctic warming, *AMBIO*, *41*(Supplement 3), 281–291.

Nakano, T., S. Kuniyoshi, and M. Fukuda (2000), Temporal variation in methane emission from tundra wetlands in a permafrost area, northeastern Siberia, *Atmos. Environ.*, *34*, 1205–1213.

Nobrega, S., and P. Grogan (2007), Deeper snow enhances winter respiration from both plant- associated and bulk soil carbon pools in birch hummock tundra, *Ecosystems*, *10*, 419–431.

Oberbauer, S. F., et al. (2007), Tundra CO_2 fluxes in response to experimental warming across latitudinal and moisture gradients, *Ecol. Monogr.*, *77*, 221–238.

Päivänen, J. (1973), Hydraulic conductivity and water retention in peat soils, *Acta For. Fenn.*, *129*, 1–70.

Parmentier, F. J. W., M. K. van der Molen, J. van Huissteden, S. A. Karsanaev, A. V. Kononov, D. A. Suzdalov, T. C. Maximov, and A. J. Dolman (2011), Longer growing seasons do not increase net carbon uptake in the northeastern Siberian tundra, *J. Geophys. Res.*, *116*, G04013, doi:10.1029/2011JG001653.

Ping, C. L., J. G. Bockheim, J. M. Kimble, G. J. Michaelson, and D. A. Walker (1998), Characteristics of cryogenic soils along a latitudinal transect in Arctic Alaska, *J. Geophys. Res.*, *103*, 28,917–28,928, doi:10.1029/98JD02024.

Rennermalm, A. K., H. Soegaard, and C. Nordstroem (2005), Interannual variability in carbon dioxide exchange from a high Arctic fen estimated by measurements and modeling, *Arctic Antarct. Alp. Res.*, *37*(4), 545–556.

Richardson, A. D., et al. (2006), A multi-site analysis of random error in tower-based measurements of carbon and energy fluxes, *Agric. For. Meteorol.*, *136*, 1–18.

Saxton, K. E., W. J. Rawls, J. S. Romberger, and R. I. Papendick (1986), Estimating generalized soil-water characteristics from texture, *Soil Sci. Soc. Am. J.*, *50*(4), 1031–1036.

Sharp, E. D., P. F. Sullivan, H. Steltzer, A. Z. Csank, and J. M. Welker (2013), Complex carbon cycle responses to multi-level warming and supplemental summer rain in the high Arctic, *Global Change Biol.*, *19*, 1780–1792.

Stewart, K. J., D. Coxson, and P. Grogan (2011), Nitrogen inputs by associative cyanobacteria across a low Arctic tundra landscape, *Arctic Antarct. Alp. Res.*, *43*(2), 267–278.

Ström, L., and T. R. Christensen (2007), Belowground carbon turnover and greenhouse gas exchanges in a sub-Arctic wetland, *Soil Biol. Biochem.*, *39*, 1689–1698.

Sturtevant, C. S., and W. C. Oechel (2013), Spatial variation in landscape-level CO_2 and CH_4 fluxes from Arctic coastal tundra: Influence from vegetation, wetness, and the thaw lake cycle, *Global Change Biol.*, *19*, 2853–2866, doi:10.1111/gcb.12247.

Sturtevant, C. S., W. C. Oechel, D. Zona, Y. Kim, and C. E. Emerson (2012), Soil moisture control over autumn season methane flux, Arctic Coastal Plain of Alaska, *Biogeosciences*, *9*, 1423–1440.

Tagesson, T., M. Mölder, M. Mastepanov, C. Sigsgaard, M. P. Tamstorf, M. Lund, J. M. Falk, A. Lindroth, T. R. Christensen, and L. Ström (2012), Land-atmosphere exchange of methane from soil thawing to soil freezing in a high-Arctic wet tundra ecosystem, *Global Change Biol.*, *18*, 1928–1940, doi:10.1111/j.1365-2486.2012.02647.x.

Tuomi, M., P. Vanhala, K. Karhu, H. Fritze, and J. Liski (2008), Heterotrophic soil respiration—Comparison of different models describing its temperature dependence, *Ecol. Model.*, *211*, 182–190.

Vourlitis, G. L., Y. Harazono, W. C. Oechel, M. Yoshimoto, and M. Mano (2000), Spatial and temporal variations in hectare-scale net CO_2 flux, respiration and gross primary production of Arctic tundra ecosystems, *Funct. Ecol.*, *14*, 203–214.

Walter, B. P., and M. Heimann (2000), A process-based climate-sensitive model to derive methane emissions from natural wetlands: Application to five wetland sites, sensitivity to model parameters, and climate, *Global Biogeochem. Cycle*, *14*, 745–765.

Wille, C., L. Kutzbach, T. Sachs, D. Wagner, and E.-M. Pfeiffer (2008), Methane emission from Siberian Arctic polygonal tundra: Eddy covariance measurements and modeling, *Global Change Biol.*, *14*, 1395–1408, doi:10.1111/j.1365-2486.2008.01586.x.

Williams, M., W. Eugster, E. B. Rastetter, J. P. Mcfadden, and F. S. Chapin Iii (2000), The controls on net ecosystem productivity along an Arctic transect: A model comparison with flux measurements, *Global Change Biol.*, *6*, 116–126, doi:10.1046/j.1365-2486.2000.06016.x.

Wilson, K. B., et al. (2002), Energy balance closure at FLUXNET sites, *Agric. For. Meteorol.*, *113*, 223–243.

Wilson, K. S., and E. R. Humphreys (2010), Carbon dioxide and methane fluxes from Arctic mudboils, *Can. J. Soil Sci.*, *90*, 441–449.

Zhu, X., Q. Zhuang, X. Gao, A. Sokolov, and C. A. Schlosser (2013), Pan-Arctic land–atmospheric fluxes of methane and carbon dioxide in response to climate change over the 21st century, *Environ. Res. Lett.*, *8*, 045003, doi:10.1088/1748-9326/8/4/045003.